EFFECTS OF MICROWAVE RADIATION ON PROPERTIES OF POLYVINYL ALCOHOL - CARBON NANOTUBE - HYDROXYAPATITE BLENDS

LIM LEE SHYAN

A project report submitted in partial fulfilment of the requirements for the award of Bachelor of Engineering (Hons.) Chemical Engineering

Lee Kong Chian Faculty of Engineering and Science
Universiti Tunku Abdul Rahman

September 2018

DECLARATION

I hereby declare that this project report is based on my original work except for citations and quotations which have been duly acknowledged. I also declare that it has not been previously and concurrently submitted for any other degree or award at UTAR or other institutions.

Signature : _____

Name : Lim Lee Shyan

ID No. : 1302230

Date : _____

APPROVAL FOR SUBMISSION

I certify that this project report entitled **"EFFECTS OF MICROWAVE RADIATION ON PROPERTIES OF POLYVINYL ALCOHOL - CARBON NANOTUBE - HYDROXYAPATITE BLENDS"** was prepared by **LIM LEE SHYAN** has met the required standard for submission in partial fulfilment of the requirements for the award of Bachelor of Engineering (Hons.) Chemical Engineering at Universiti Tunku Abdul Rahman.

Approved by,

Signature : _____

Supervisor : Dr. Bee Soo Tueen

Date : _____

ACKNOWLEDGEMENTS

I would like to thank everyone who had contributed to the successful completion of this project. I would like to express my gratitude to my research supervisor, Dr. Bee Soo Tueen for her invaluable advice, guidance and her enormous patience throughout the development of the research.

In addition, I would also like to express my gratitude to my loving parents and friends who had helped and given me encouragement as I were conducting my research.

EFFECTS OF MICROWAVE RADIATION ON PROPERTIES OF POLYVINYL ALCOHOL - CARBON NANOTUBE - HYDROXYAPATITE BLENDS

ABSTRACT

This study is aiming to investigate the effects of microwave radiation on properties of polyvinyl alcohol-carbon nanotube- hydroxyapatite blends. CNT and HAP with different loading level were added to PVOH matrix and 150 W microwave radiation were applied on polymer nanocomposites. Adding both CNT and HAP fillers with high loading level increased the tensile strength of PVOH blends. Incorporation of HAP decreased the Young's modulus but incorporation of CNT increased the Young's modulus of polymer blends. Addition of CNT or HAP decreased the elongation at break of polymer nanocomposites. The application of microwave radiation improved tensile strength, Young's modulus, and also elongation at break of polymer blends. As both fillers were added at high amount, the melting temperature and enthalpy of melting increased. Microwave radiation for polymer blends with high loading level of CNT and HAP increased the melting temperature and enthalpy of melting. For SEM analysis, flakes were presented for polymer nanocomposites with high loading of filler due to agglomeration and microwave radiation reduced the amount of fibrils on the fracture surface of PVOH blends. XRD results show the dispersion of filler on polymer nanocomposites and crystallinity of PVOH blends. Increment of CNT, HAP and application of microwave radiation decreased the crystallite size and crystallinity of polymer nanocomposites. Different vibration of functional groups were observed for the three materials (PVOH, CNT, and HAP). Thermal degradation is classified into three stages from TGA analysis. Sufficient addition of fillers on polymer blends improves the thermal stability. Application of microwave radiation at low loading CNT added polymer blends increased the thermal stability.

TABLE OF CONTENTS

LIST OF TABLES

LIST OF FIGURES

LIST OF SYMBOLS / ABBREVIATIONS

d	d-spacing
K	Scherrer constant
kGy	Gray, $\frac{m^2}{s^2}$
L	crystallite size
phr	part per hundred rubber
R	interchain separation
W	power (Watt)
β	full width at half maximum (FWHM) of deflection peak
θ	Bragg angle, radians
λ	1.542Å

ACS	acetylated starch
CNC	cellulose nanocrystals
CNT	carbon nanotube
CS	corn starch
CSV	cassava starch
CVD	chemical vapour deposition
DAS	dialdehyde starch
DSC	Differential Scanning Calorimetry
FTIR	Fourier Transform Infrared
HAP	hydroxyapatite
HDPE	high density polyethylene
LDPE	low density polyethylene
MMT	montmorillonite
MWCNT	multi-wall carbon nanotube
MWR	microwave radiation
PP	polypropylene
PPV	plasticized PVOH
PVOH	polyvinyl alcohol
RPP-PSP	recycled polypropylene and peanut shell powder
SEM	Scanning Electron Microscopy

SWCNT	single-wall carbon nanotube
TEM	Transmission Electron Microscopy
TGA	Thermogravimetric Analysis
XRD	X-ray Diffraction

CHAPTER 1

INTRODUCTION

1.1 General Introduction

The disposition of plastic wastes was a serious problem. Majority of plastic materials such as polystyrene and polypropylene are manufactured from petroleum sources. However, this kind of materials are non-biodegradable after disposing in the natural environment. Thus, researchers came out alternative methods to manufacture polymeric products from natural compounds such as starches, proteins, and lipids (Avérous, 2008)

A biodegradable polymer can be from the source of synthetic or natural polymer that is likely to degrade to smaller components and natural by-products in the presence of enzyme or microorganisms (Gooch, 2010). Although non-degradable polymers have brought some advantages, their resistance to the degradation process leads to the high accumulation speed of plastic wastes in the environment. Biopolymers have been studied and utilized to solve the disposal issue of petroleum-based polymers. In order to replace the petroleum-based plastics, thermal properties mechanical properties, and functions of biopolymers have to be improved (Chavan, 2015).

The development of bio-nanocomposites helps improve the properties of biopolymer (Yao, 2010). Nanocomposites consist of more than one component which can be matrix and filler, and one of the component is in nanoscale (< 100 nm) (Ishida, 2000). There are three kinds of nanocomposites including ceramic nanocomposites, metal nanocomposites, and polymer nanocomposites in which the matrix is ceramic, metal, and polymer respectively. Polymeric nanocomposites have been widely used owing to their improved properties as compared to pure polymers (Han & Fina, 2011). These improved properties can be achieved with the use of extremely low amount of nanofiller in contrast with the higher content in conventional composites (Chavan, 2015).

The developing demand for eco-friendly products results in replacement of synthetic fillers with natural cellulose-based fillers. The nanocomposites are produced by blending natural organic fillers with polymers (Zaaba, et al., 2016).

1.2 Problem Statement

Polyvinyl alcohol (PVOH) is a biodegradable polymer used in extensive applications such as papermaking, textiles and printing industries and can be used as pharmaceutic aid, ophthalmic lubricant and used in the production of cosmetics, surface coatings artificial sponges, and other products. However, the purchasing price of polyvinyl alcohol is very high. This can be solved by incorporating carbon nanotube (CNT) and hydroxyapatite (HAP) extracted from the shell of hard clam in polyvinyl alcohol matrix to enhance the mechanical and thermal properties of polyvinyl alcohol. Other than that, the radiation by microwave would also affect the properties of polyvinyl alcohol. Therefore, this research is performed to evaluate the consequence of microwave radiation on PVOH-HAP-CNT blends. Following are the problem statement for this study:

1. What are the mechanical properties and thermal properties of different composition of PVOH-HAP-CNT blends?
2. What are the mechanical properties, thermal properties, and physical properties of PVOH-HAP-CNT blends under different dose of microwave radiation?

1.3 Aims and Objectives

The objectives of this study are to investigate the interaction effect between polyvinyl alcohol, hydroxyapatite and carbon nanotube by evaluating the characteristics of the PVOH-HAP-CNT blends and obtaining the optimum composition of polyvinyl alcohol, hydroxyapatite and carbon nanotube in the blends and radiated PVOH-HAP-CNT blends. In order to achieve the main objectives, sub-objectives are identified as follows:

1. To evaluate the mechanical and thermal properties of PVOH-HAP-CNT blends.
2. To observe the surface morphologies and microstructure of the blends.
3. To investigate the consequences of microwave radiation on mechanical properties, thermal properties, and physical properties of PVOH-HAP-CNT blends.

1.4 Scope and Limitation of the Study

This study mainly focuses on the preparation and characterization of PVOH-HAP-CNT blends. Blends of of polyvinyl alcohol, hydroxyapatite and carbon nanotube were prepared at different composition. The samples were compounded to specimen with

the use of casting method. Several tests were carried out to characterize the PVOH-CNT-HAP blends.

1.4.1 Mechanical Properties

Tensile test was conducted to measure elongation at break, tensile strength, and Young's modulus of PVOH-CNT-HAP blends. The tensile test was carried out in accordance to ASTM D882 standard.

1.4.2 Thermal Properties

The onset, endpoint melting temperature, and melting enthalpy of the blends were obtained from the Differential Scanning Calorimetry (DSC) test.

1.4.3 Physical Properties and Morphologies

Scanning Electron Microscopy (SEM) was conducted to determine the morphology of PVOH-CNT-HAP blends. X-ray Diffraction (XRD) was used to study the crystallinity and dispersion of hydroxyapatite and carbon nanotube on the PVOH matrix.

1.4.4 Chemical Interactions and Bonding

Fourier Transform Infrared (FTIR) was used to identify chemical features and shifts that occur because of the interactions between functional groups of the blended specimen. FTIR generated an infrared spectral scan of the sample that absorbs infrared light.

1.4.5 Thermogravimetric Analysis

Thermogravimetric Analysis (TGA) was carried out to measure the change in weight of samples over a range of temperature, time and atmosphere.

CHAPTER 2

LITERATURE REVIEW

2.1 Polyvinyl Alcohol (PVOH)

2.1.1 Properties of Polyvinyl Alcohol

Polyvinyl alcohol (PVOH) is a hydrophilic polymer attached with hydroxyl group on every repeating unit, which allows the formation of hydrogen bonding between PVOH and carboxyl and hydroxyl groups of cellulose fillers (Zaaba, et al., 2016). Polyvinyl alcohol is a semi-crystalline and water-soluble synthetic polymer with good biodegradability, chemical resistance and mechanical properties due to the presence of hydroxyl groups and the ability in hydrogen bond formation. It is a highly hygroscopic polymer and this characteristics may weaken its mechanical properties and restricting its use for some intended applications (Dorigato & Pegoretti, 2011).

Polyvinyl alcohol has a high degree of crystallinity as a result of the small sized hydroxyl group that can suit into the lattice structures induces the constitution of high oriented crystalline structures. Polyvinyl alcohol can be categorized into two groups, fully hydrolysed PVOH and partially hydrolysed polyvinyl alcohol. The fully hydrolysed PVOH has higher crystallinity in contrast to partially hydrolysed PVOH because of the existence of strong hydrogen bond that able to hold the chains together. The strong hydrogen bonds impede the mobility of the chains within the polymer matrix, thus exhibiting higher rigidity and strength. The highly crystalline material that promotes stronger mechanical properties is more desirable as compared to the less crystalline material (Rwei & Huang, 2012).

2.1.2 Comparison between Polyvinyl Alcohol and Other Polymers

Polyvinyl alcohol is different from the commodity thermoplastics such as polystyrene and polyethylene which their degradation temperatures are far away from their melting temperatures of more than 50 ℃ (Kholodovych & Welsh, 2007). The commodity thermoplastics have very little possibilities to undergo thermal degradation when melting. However, PVOH without adding plasticizer has a melting point very near to its degradation temperature. PVOH likely to degrade during the melt processing stage by producing yellowish output (Wang, et al., 1998).

2.1.3 Applications of Polyvinyl Alcohol

Polyvinyl alcohol is synthetic polymer that is used in extensive medical, industrial, commercial, and food applications such as surgical threads, resins, lacquers, and food-contact packaging due to the degradation ability, resource-saving production process using non-petroleum route, soluble-in-water property, chemical resistance and gas barrier properties (DeMerlis & Schoneker, 2003).

Polyvinyl alcohol has been widely applied for the fabrication of blends and composites with other natural and renewable polymers. PVOH film exhibits excellent physical properties but it is expensive and its biodegradation rate is relatively low (Chiellini, et al., 2003). In order to reduce the price and increase the rate of biodegradation, film casting has been introduced by blending water solutions of starch (Azahari, et al., 2011). Inorganic fillers can also be incorporated in polymer composites as reinforcing agents to improve the properties of polymer composite.

2.1.4 Polyvinyl Alcohol in Polymer Nanocomposite

According to Lee, et al. (2011), neat cassava starch (CSV) has higher thermal resistance than neat PVOH because of the cyclic hemiacetal structure in starch that is sustainable to thermal attacks. Blending of cassava starch with PVOH dramatically increases the thermal stability of PVOH. PVOH with CSV at blending composition of 40 and 50 wt% have the highest activation energies compared to other blending compositions. This proved that PVOH-CSV blends are synergistically compatible.

A research by Lee, et al. (2010) concluded that blending of plasticized PVOH (PPV) affects the processing properties and viscosity of cassava starch. The reciprocal actions between PVOH and starch are strong and stimulate the exercise of starch molecules when the polymer nanocomposite is exposed to shear force. The addition of CSV reduces the crystallinity of PPV owing to lower transition of specific volume at molten stage.

Cataldi, et al. (2018) showed that the addition of cellulose nanocrystals (CNC) improves the thermal stability of neat PVOH, enhances storage and loss modulus of polymer within the range of temperature examined. Cellulose nanocrystal allows the suppression of rubber-like behaviour in polyvinyl alcohol. Two weight percent of cellulose nanocrystal in nanocomposite improves tensile energy up to 85% and stress at break up to 45 %.

In research conducted by Katerinopoulou, et al. (2014), the substitution of glycerol with PVOH in the acetylated starch-polyvinyl alcohol-clay (ACS-PVOH-MMT) system gains superior mechanical strength owing to the formation of hydrogen bonding between ACS and PVOH matrix. Blending of PVOH with ACS and glycerol improves storage modulus and glass transition temperature attributed to the hydrogen bond creation and the intercalation of NaMMT with polymer matrix. The nanocomposite induces significant reduction in water vapour permeability, approximately 67 % for acetylated starch-polyvinyl alcohol-clay nanocomposites compared to thermoplastic acetylated corn starch.

Based on research by Giannakas, et al. (2016), the introduction of PVOH to chitosan based film acts as plasticizer that causes higher strain at break, lower stiffness and strength, enhanced water and oxygen barrier, but has no significant effect on antimicrobial activity.

Results from research of Recycled Polypropylene and Peanut Shell Powder Composites (RPP-PSP) showed that the addition of PVOH into RPP-PSP composites improves mechanical properties such as tensile strength, water absorption, Young's modulus, elongation at break, and better interfacial adhesion (Zaaba, et al., 2016).

2.2 Carbon Nanotube (CNT)

2.2.1 Properties of Carbon Nanotube

Carbon Nanotube (CNT) has excellent property of one-dimensional (1D) species of a pure sp^2-hybridized hexagonal carbon nano-particle. This results in enhancement of the mechanical properties and physical properties of polymers. Carbon nanotubes are mechanically stable, electrically and thermally conductive, and possess extremely high stiffness. Based on the nano-diameter of nanotube, they have an exceptionally large surface area. (Fiedler & Schulte, 2018). Single-wall carbon nanotube (SWCNT) and multi-wall carbon nanotube (MWCNT) are two types of carbon nanotube available.

Based on the low density and high aspect ratio, carbon nanotube has excellent results in enhancing the thermal, electrical, and mechanical properties of polymer nanocomposite comparing to pristine polymer (Aboutalebi, 2012). There are several methods for the manufacturing of carbon nanotube such as chemical vapour deposition (CVD), laser ablation, arc discharge, carbon monoxide disproportionation, and hydrothermal method (Kumari, 2014).

2.2.2 Structure of Carbon Nanotube

Figure 2.1 shows the range of diameters for different materials. Carbon nanotube possesses various diameters, lengths, and number of cylindrical shells due to the production process. Besides the difference in geometry, the differences in density of lattice defects, chirality, and side groups result in different electrical conduction, stiffness, strengths, and interactions with the polymer matrix. All these aspects affect the processing of carbon nanotube such as the dispersion and percolation in polymer matrix. Factors including specific surface interaction, temperature, and convection at the liquid state of polymer affect the morphology of the network (Martin, et al., 2004).

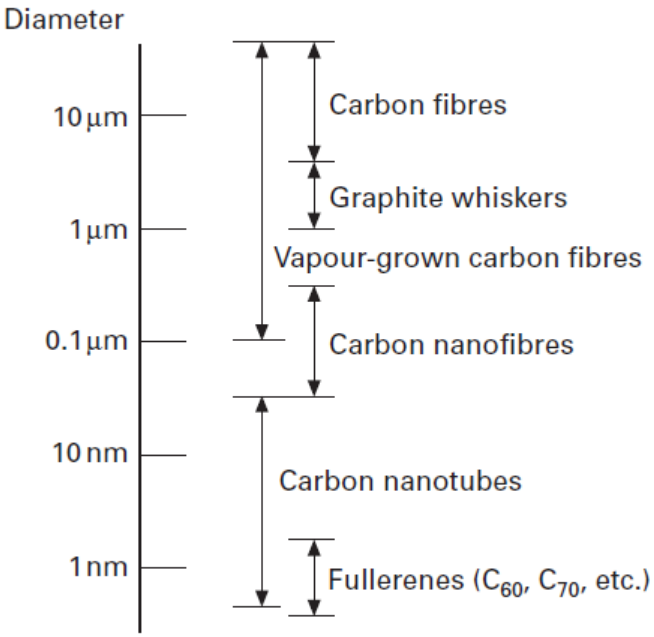

Figure 2.1: The Diameters for different Carbon-Based Materials (Shaffer & Sandler, n.d.)

2.2.3 Application of Carbon Nanotube

Carbon Nanotube has attracted a lot attention due to its exceptional physicochemical, mechanical, electrical, optical, and thermal properties (Eckel, 2004) (Merino, 2015). Carbon Nanotube that functions as filler in a polymeric matrix improve the mechanical properties such as the fracture behaviour, and electrical conductivity (Fiedler & Schulte, 2018). Thus, it is used in many application such as hydrogen storage, drug

shipment, chemical sensor (Bianco, 2005), and reinforcement applications in nanocomposites (Merino, 2015).

Polymer-sheathed carbon nanotube is used to various sensing applications as a result of its huge specific surface area and great electrical properties (Aussawasathien, et al., 2006). Aligned CNT painted with conducting polymers can be applied in glucose and complementary-DNA sensors with high incisiveness and selectivity. The increment in crystallinity as a result of the existence of nanotubes raises a favourable effect in the mechanical properties of the polymer composites. MWCNT-PVOH composite is designed to fit specific requirement of diverse applications such as filters of tuneable pore size, components of composite panel and sensor applications (Dassios & Galiotis, 2012).

2.2.4 Dispersion of Carbon Nanotube

Carbon nanotubes are multifunctional reinforcements that can enhance the thermal, mechanical and electrical properties of polymer nanocomposite. However, the dispersion of carbon nanotube to polymer matrix is troublesome thus restricting the potential advantages that can be proposed by carbon nanotube (Sandler, et al., 2003) The procedures used to enhance the scattering of CNT in polymer matrix are functionalization of chemical, cutting of the carbon nanotube, in situ polymerization, and improved physical blending (Xie, et al., 2005). Another alternative method by mixing carbon nanotubes directly into the matrix is to join the carbon nanotubes to host particles before adding into the resin. This method bring about the production of hierarchical composites such as carbon-glass fibre-nanotube composites where the carbon nanotubes has higher z-plane stiffness, stronger fibre-matrix interface and can be used as large surface area electrodes (Qian, et al., 2010). Besides, attaching the carbon nanotubes to host particle does not significantly increase the viscosity of the system (Othman, et al., 2013).

2.2.5 Carbon Nanotube in Polymer Nanocomposite

According to Park & Lee (2018), polyvinyl alcohol can be used as a binder connecting the carbon nanotube via hydrogen bond formation in the blending. This bond formation provides the formation of intermolecular bonds between carbon nanotubes where PVOH acts as a medium to join the individual carbon nanotubes to form an

interconnected structure. The composite structure promotes improved mechanical properties.

The incorporation of carbon nanotube in polyvinyl alcohol produces polymer composite of advanced mechanical and electrical properties comparing to the pure polymer. Carbon nanotube able to act as nucleating agents for PVOH crystals and can increase the crystallinity of PVOH in polyvinyl alcohol-carbon nanotube (PVOH-CNT) composite (Shaffer & Windle, 1999).

Ryan, et al. (2007) reported that Young's modulus of a semi-crystalline polymer, polyvinyl alcohol increased 4.5 fold with the introduction of carbon nanotubes. The polymer crystallinity is observed to increase for PVOH-CNT blends because increase in Young's modulus and tensile strength affect the mechanical properties of the polymer nanocomposite. Carbon nanotube with considerably small diameter is applied in variety of reinforcement applications since crystallinity of the semi-crystalline polymer has improved.

In the research conducted by Dassios & Galiotis (2012), Scanning Electron Microscopy (SEM) and Transmission Electron Microscopy (TEM) imaging shows that polymer sheathing attached uniformly over the nanotubes in the mats with no change in their surface morphology, alignment or physical properties.

Another research is carried out by Wongon, et al. (2016) whereby scanning electron microscopy photographs reveals that the polyvinyl alcohol-multiwalled carbon nanotube (PVOH-MWCNT) composite nanofibers are smooth with no bead exists in the composite nanofibers. The addition of multiwalled carbon nanotube helps improving thermal property of the Low Density Polyethylene (LDPE) owing to the resistance to thermal action and the presence of scavenging free radicals (Yang, et al., 2015)

2.3 Hard Clam (HC)

2.3.1 Introduction of Hard Clam

Clam is food with lot of nutrient in it. Clams such as hard clam (Meretrix meretrix) consist of enzymes, peptides, proteins, polysaccharides, mineral, essential vitamins, and essential amino acids which are contributed for its nutritive and medical functions (Xie, et al., 2012). The hard clam, Marcenaria mercenaria has 91.8 % of moisture, 4.41 % of protein, 1.97 % of ash, 0.21 % of fat and is rich in mineral (Sidwell, et al.,

1973). Asian hard clam with its scientific name, Meretrix lusoria is an general bivalve located in East and Southeast Asia (Yoosukh & Matsukuma, 2001). This clam is served as crucial distribution of shellfish in areas such as Japan, Korea and China and the cultivation technology for this type of clam is developing (Chung, 2007). However, this hard clam does not have the large usage in Thailand due to the presence of large amount of mucus and tough texture of clam. Because of the little market value in association with the small demand in consumption, it is acted as alternate source of baby clam (Cardiidae) in canned seafood industries, basic material in shrimp industries (Karnjanapratum, et al., 213).

2.3.2 Composition of Hard Clam

The portion of clam is then dissected into three section comprising the foot, mantle, and viscera containing 36.07 %, 45.45 %, and 18.48 % of edible portion respectively. This composition of the three portions of clam is shown in Table 2.1. The results indicates that hard clam from the Andaman-Sea coast consists abundant nutrients such as proteins, fats, and minerals (Karnjanapratum, et al., 213).

Table 2.1: Compositions of the Three Portions of Asian Hard Clam (Karnjanapratum, et al., 213)

Portions	Compositions (%)				
	Moisture	Protein	Carbohydrate	Fat	Ash
Foot	76.23 ± 0.09c	12.75 ± 0.42a (54.63 ± 0.65)B	7.89 ± 0.05a (33.55 ± 0.57)A	1.58 ± 0.00c (6.64 ± 0.00)C	1.23 ± 0.02c (5.18 ± 0.08)C
Mantle	84.22 ± 0.06a	9.09 ± 0.27c (57.55 ± 1.73)A	1.20 ± 0.15b (7.78 ± 0.91)B	3.53 ± 0.06b (22.36 ± 0.38)B	1.94 ± 0.03b (12.30 ± 0.17)B
Viscera	80.89 ± 0.11b	9.61 ± 0.63b (49.27 ± 0.92)C	0.32 ± 0.04c (3.54 ± 0.60)C	6.58 ± 0.2a (33.68 ± 0.09)A	2.58 ± 0.08a (13.50 ± 0.77)A

2.3.3 Environmental Issues of Seashell

Seashells of bivalves are an aquaculture by-product as a result of large consumption and this leads to serious solid waste problem. Manufacturing industries produce large amounts of sea wastes such as mussels, clams, barnacles, scallops and oysters. Accumulation of seashell wastes such as cockles, wedge-shells and other small bivalve shells in the seashores is also a problem especially after storms (Fombuena, et al., 2014). This seashell waste able to utilize as bio-filler for polymer matrix because it has same composition as conventional calcium carbonate. Basically, calcium carbonate is used as inorganic filler due to its cheap cost and the ability to enhance mechanical

properties such as stiffness and dispersion of particle in polymer matrix (Doufnoune, et al., 2003).

2.3.4 Seashell in Polymer Nanocomposite

The study that was carried out by Fombuena, et al. (2014) stated that the calcium carbonate from seashell is a bio-filler and can be used with matrix to manufacture materials with large amount of renewable materials. The high thermal stability and wide range of availability of seashell allow seashell to be used as ideal filler in composite so as to decrease material costs and improve the mechanical and thermal properties of composite. By adding 30 wt% of seashell bio-filler, the flexural modulus can increase over 50% which can be attributed to excellent filler-matrix interaction. The introduction of calcium carbonate from seashell wastes increases the glass transition temperature, T_g and thermal stability of polymer matrix (Fombuena, et al., 2014).

From a study conducted by (Xia, et al., 2014), shell waste which possesses high content of calcium carbonate and organic matrices able to be used as biofiller. The alteration on surface due to addition of biofiller improves the compatibility between the modified clam shell and the polypropylene (PP) matrix, hence improving thermal stability. Strong reciprocal action between modified clam shell and the polypropylene increases significantly in the mechanical properties of polypropylene composite. Other than that, the modified clam shell is at low cost and environmentally friendly. Differential scanning calorimetry indicates that the modified clam shell powder able to act as a nucleating agent that increases the crystallization temperature of polypropylene (Yao, et al., 2013).

2.4 Hydroxyapatite (HAP)

2.4.1 Introduction of Hydroxyapatite

Hydroxyapatite (HAP), $Ca_{10}(PO_4)_6(OH)_2$ ceramics are popular for application in bone grafting owing to their good osteo-conductive and bioactive properties (Wang, et al., 2013). Hydroxyapatite nanostructures can extensively improve the bio-affinity and bioactivity of synthesized biomaterial (Sanosh , et al., 2010). Hydroxyapatite powders are often extracted using bio-waste products such as egg shells, corals, cuttlefish shells, bovine bone, and others to satisfy the demands in developing green technologies. Bio-

waste products are sources that are rich of calcium carbonate and calcium oxide. One of such bio-waste which is composed of calcium carbonate and calcium oxide is clam shells. The clam shell contributes about 70 wt% of shell fish waste generated in worldwide. Extraction of hydroxyapatite from clam shell are highly beneficial because it is cheap and plentiful in nature.

2.4.2 Production of Hydroxyapatite

Clam shell is used for manufacturing hydroxyapatite powder. For example, calcium precursors derived from the clam shell hydrothermally synthesize dense hydroxyapatite structures at 200 ℃ (Vecchio , et al., 2007). This is a promising technique for the production of pure hydroxyapatite, however the hydroxyapatite structure need post machining to acquire desired shapes for implantation. Another research reported by (Gunduz , et al., 2014), clam shells are used to synthesize hydroxyapatite powders at 800 ℃. The constraint of this technique is poor control over the particle size.

2.4.3 Hydroxyapatite in Polymer Nanocomposite

According to Mohammadi, et al. (2017), the crosslinking density increases with the increase in absorbed dose of electron beam irradiation and percentage of nano-hydroxyapatite added in composites in the hot-set and gel content test. In Differential Scanning Calorimetry (DSC) diagram, the crystallinity peak area in the nano-High Density Polyethylene-hydroxyapatite (HDPE-HAP) composite is higher than composite prepared using high density ethylene granules only. This can be considered an indication of excellent dispersion of the reinforcement phase. The researchers state that preparation of the nano-composites by synthesizing nano-polymer can reduce the agglomeration problem.

The results from Soltani , et al. (2013) shows that increase in the amount of hydroxyapatite nano-particles added bring about an increment in the crosslinking density of the composite. Increasing the percentage of hydroxyapatite nano-particle in the composite results in an increase in crystallinity but decrease after reaching the critical percentage of hydroxyapatite nano-particle. The addition of hydroxyapatite will also affect the mechanical properties of polyethylene-hydroxyapatite (PE–HAP) nanocomposite due to the rigidity of the reinforcing filler (HAP). The filler is brittle and it promotes unsatisfied interfacial adhesion to the polymer matrix at the condition

of larger stress in break point. Upon this condition, the polyethylene-hydroxyapatite interface functions as zone of stress concentrator making the polymer composite fragile.

2.5 Microwave Radiation (MWR)

2.5.1 Introduction of Microwave Radiation

Microwave radiation is known as non-ionizing radiation that creates heat inside penetrated medium by friction of molecule in alternative electromagnetic field. The design of microwave processing is mandatory to include thermal properties of the product to be processed and electrical properties which vary with the operating frequency and time-temperature profile of the product (Lewandowicz, et al., 1997).

Microwave is electromagnetic wave in the frequency range of 300 MHz-300 GHz. Microwave transmission is polarized radiation and it is horizontal or vertical orientation to the substrate under adsorption. Microwaves can be transported through air and water in long distance. Microwave radiation generates efficient internal heat-transfer, leads to consistent heating on the sample as compared to wall heat-transfer through thermal heating (Weerakkody, et al., 2018).

2.5.2 Application of Microwave Radiation

Microwave radiation can be used to synthesize and process polymeric materials. It is a fast and highly efficient method of thermosetting resin crosslinking, scattering of polymers and resins, emulsion polymerization of vinyl monomers, and instant drying on aqueous solutions. Microwave radiation is widely applied for continuous vulcanization of extruded rubber, and vulcanization of rubber intermittent in molds. Rubber vulcanization improves product homogeneity, reduces the cross linking time and waste production as compared to commercial vulcanization in autoclave steam and hot air. Other than that, microwave radiation is employed in organic chemistry and polymers chemistry as it able to reduce the synthesis time and energy, and decrease or fully eliminate the usage of volatile and flammable solvents which are not required in production of biomedical polymers such as polyurethanes. (Lipka, et al., 2017).

2.5.3 Advantages and Disadvantages of Application of Microwave Radiation

Application of microwave radiation in polymer processing proposes few advantages when comparing to commercial processing methods. Extremely uniform temperature profiles can be observed in the processing of polymer as the penetration depth of microwave radiation in most polymer materials is large (about 30 cm or more). This brings about decrement of residual stresses that is formed due to the reason of non-uniform processing. Microwave radiation is allowed to achieve faster heating rate and uniform thermal distribution at the same time and minimize the cycle time of process. This is different from conventional process which uses slow thermal ramp rate to conduct thermal convection. Moreover, Microwave radiation promotes large amount of electrical savings during polymer processing (Lewis, n.d.).

However, preheating process of rubber weather seal in automobile industry is the only commercial application that significantly uses the microwave processing despite of all advantages proposed by microwave radiation. Microwave radiation fails to be applied in industrial market. This is due to the fact of inadequate understanding of process and insufficient instrument that operates the control level required to avoid thermal degradation of polymer being processed (Lewis, n.d.).

2.5.4 Effects of Microwave Radiation

Radiation is carried out by exposing polymer to alpha-rays, gamma-rays, X-rays, microwaves, electron beam irradiation, ultra-violet and so on. Radiation promotes cross-linking and degradation which are subjected to dosage of radiation, polymer structure, and temperature. Degradation of polymer will affect the macroscopic properties such as mechanical properties, electrical conductivity, and others. Polymer can be classified as crosslinking polymer and chain scission polymer according to the type of structural change (Somashekarappa, et al., 2013).

Microwave radiation on silk fibroin films improves the generation of polypeptide chain and therefore aids in the regeneration of structure of silk fibroin into thin film with three dimensional form. From that, it is known that the microwave irradiation allows silk fibroin protein to return its original structure and physical properties when changes into other forms depends on the application. The regeneration of silk fibroin structure makes it more brittle in nature (Mahadevaiah, et al., 2016).

Microwave radiation able to affect the temperature and moisture loss of the starches. Moisture content has very strong correlation with the increase rate of

temperature. Sample with low moisture content illustrates significant rise in temperature and vice versa (Lewandowicz, et al., 1997).

Hydrogen bonds network (physical crosslinking) is formed after microwave radiation. It is considered the most symbolic structural changes under application of microwave radiation. Hydrogen bonds determine the binding effect of moulding sands with CMS-Na binders. High amount of hydrogen bonds proposes high polarizability in the structure (Kaczmarska, et al., 2018).

Microwave radiation able to enhance the tensile strength and stiffness of polymer composites. Microwave radiation is widely applied in polymer processing. In fact, CNT is excellent microwave absorbents. Under radiation, energy can be transported from microwave field to CNT through dipole polarizations promoted by alternating electric field and mechanical vibration induced by phonon-phonon interaction. The energy then creates intense heating, outgassing, and light emission. Microwave radiation improves the interfacial bonding for nanotube composites (Qu, et al., 2018).

Microwave radiation can accelerate the reactions of the Ag^{+} ions with surface of hydroxyapatite and the rate of variation in hydroxyapatite cell unit volume. Besides, microwave radiation can modify the crystallographic feature of hydroxyapatite nanocrystals and also the doping rate of silver ion on hydroxyapatite (Simões, et al., n.d.).

With the application of short period microwave radiation, carbon fibre exhibits higher adhesion and interfacial shear strength. This evidences that microwave radiation can be used as pre-treatment for fiber since it improves the interfacial strength in short time without incorporation of others chemicals (Wang, et al., 2016).

2.6 Crosslinking and Chain Scission

Radiation of polymer may results in chain scission leading to decrement of molecular weight of macromolecules and crosslinking that causes the formation of macromolecules. The predominance of these effects depends on the polymer nature and the conditions before, during and after radiation (Relleve, et al., 2018).

Formation of crosslinking changes linear polymer into insoluble, three dimensional structures. This causes an expressive increase in molecular weight and enhancement in mechanical properties. Degradation on the other hand reduces the molecular weight and worsen the physical properties of polymer. Crosslinking and

degradation can occur simultaneously but the dominance of their rate depends on the chemical structure, physical state, and radiation state applied on polymer (Singh, et al., 2017).

At low dosage radiation, chain scission is the dominant process that occurred in highly constrained chain segments. Chain scission creates free radicals and reduces the molecular weight of polymer. Chains that are linked together to generate cross-linked agglomerates in pristine polymer are more likely to induce chain scission. As the radiation dosage is increased, the amount of free radicals formed is adequate to attack neighbouring chains, thus leading to chain branching and cross-linking (Otaguro, et al., 2010)

PVOH is widely applied to applications that undergo radiation induced polymerization and crosslinking. Radiation on polyvinyl alcohol creates two types of radicals; one by taking out hydrogen from carbon atom of CH_2 groups and the other one by abstracting oxygen of hydroxyl groups. Intermolecular crosslinking happens with another free radicals and branching begins to generate crosslinked network (Singh, et al., 2017).

2.7 Tensile Test

Tensile test is conducted to measure elongation at break, tensile strength, and Young's modulus of polymer. Figure 2.2 shows the mechanical properties under different doses of irradiation. In Figure 2.2 (a), tensile strength increases as the montmorillonite (MMT) increases at level below 1.5 phr because PVOH matrix which contains large number of hydroxyl group binds with the hydrophilic surface of MMT. When the addition of MMT increases over 2.5 phr, poor dispersion of MMT induces stress concentrator on the matrix when extension is applied (Tee, et al., 2013; Tee, et al., 2013). The usage of irradiation able to enhance the tensile energy of the PVOH–MMT because of the creation of crosslinking lattice in the polyvinyl alcohol matrix which opposes the mobility of chains. As the irradiation doses increase from 16 kGy to 36 kGy, tensile strength reduces faintly owing to the disruption of PVOH structure that is attacked by excessive free radicals upon high dose irradiation. Ahmad, et al. (2012) mentioned that chain scissioning and crosslinking existed together particularly at high dosage of irradiation. As the amount of MMT exceed 2.5 phr, the MMT distributed all over polymer matrix suppress the attacking action of free movement radicals to form

crosslinking network, this leads to decrease in tensile strength of composite upon application of electron beam application.

In Figure 2.2 (b), the results of Young's modulus show that the rigidity of 26 and 36 kGy PVOH–MMT composite containing 3.5 and 4.5 phr MMT is vaguely smaller than 0 and 6 kGy PVOH–MMT composite consisting 1.5 and 2.5 phr MMT. The flexural modulus shows the highest rigidity of PVOH–MMT at 2.5 to 3.5 phr MMT and 16 kGy irradiation. This is so because the scattering effect of montmorillonite and formation of crosslinking at this stage enhanced the structure of composite.

In Figure 2.2 (c), neat polyvinyl alcohol shows the highest elongation comparing to the others owing to the presence of entangled polymer which can move randomly when treated to expansion. Besides, the crosslinking network caused by irradiation limits the chains sliding capability. When PVOH–MMT composite is subjected to high irradiation dosages, chain scission process produces low molecular weight compound that performs as chain slider to ease the movement of polymer matrix, thus increasing elongation of polymer matrix. On the other hand, the decrement in elongation can be caused by agglomeration due to high loading level of MMT.

From another research conducted by Bee , et al. (2018), the introduction of CS and DAS into polyvinyl alcohol matrix significantly decreased the tensile energy of PVOH composites accredited to the presence of polyvinyl alcohol instead of starch in the matrix that weakens the hydrogen bonds.

According to Mohammadi, et al. (2017) in Figure 2.3, it shows the Young's modulus of polymer composite under different irradiation dose. By increasing the nano-structure hydroxyapatite (HAP), the Young's modulus of polymeric composite will be increased. This indicates that nano-high density polyethylene (HDPE) exhibits better mechanical properties than normal granules of HDPE. This is because more surface of contact between matrix and filler in HDPE-HAP nano-composite increases the van der Waals interactions, therefore improving the strength of the nano-composite.

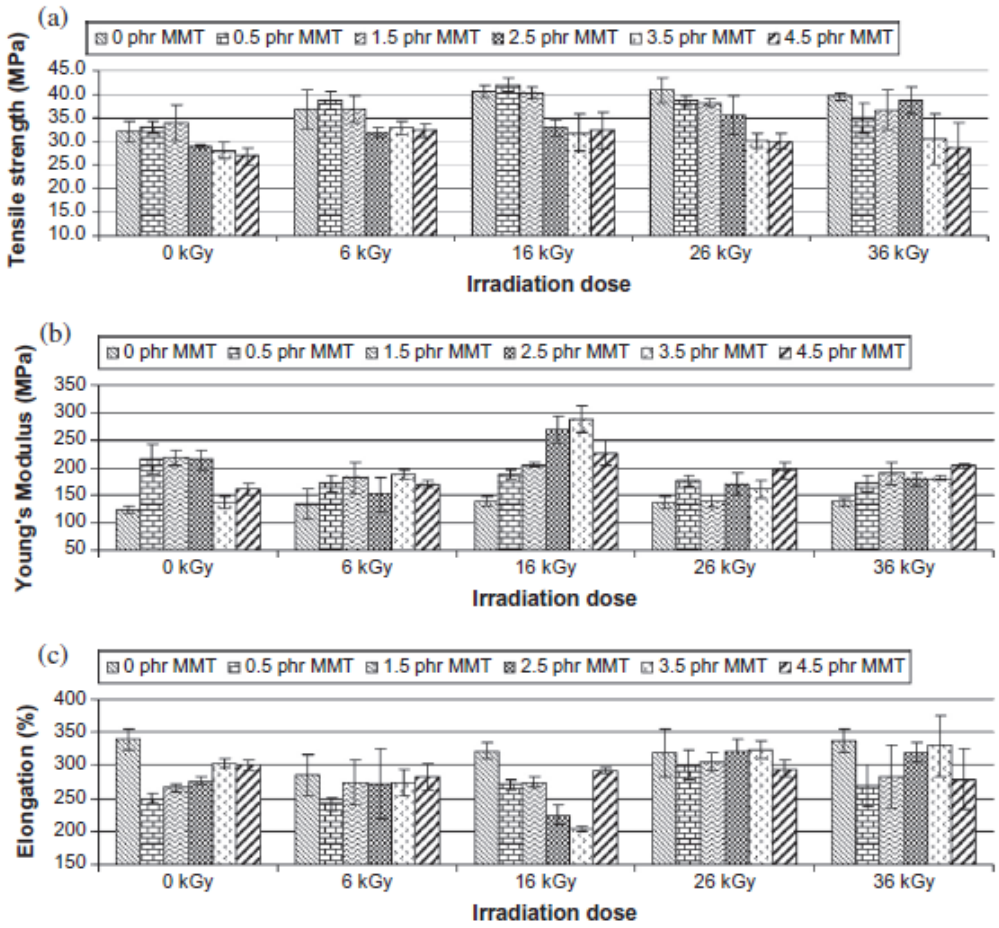

Figure 2.2: (a) Tensile Energy, (b) Flexural Modulus and (c) Elongation at Break for Polyvinyl Alcohol– Montmorillonite Composite under different irradiation doses (Bee, et al., 2014)

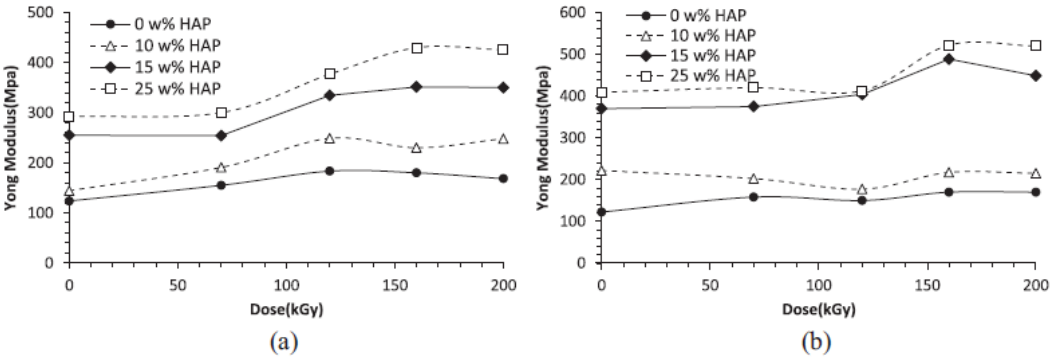

Figure 2.3: Young's Modulus against Irradiation Doses of (a) HDPE-HAP and (b) Nano-HDPE-HAP (Mohammadi, et al., 2017)

2.8 Differential Scanning Calorimetry (DSC)

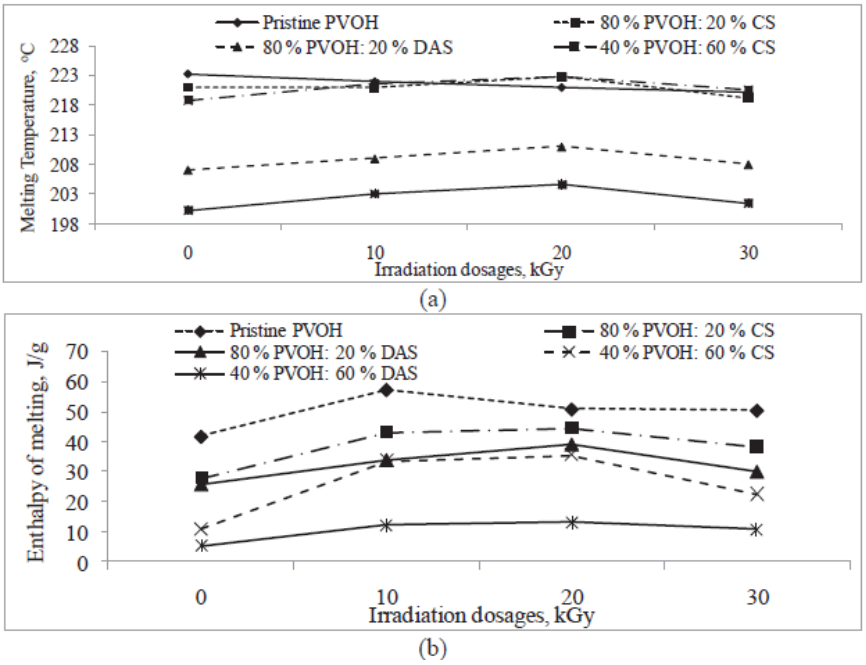

Figure 2.4: Consequence of Irradiation on the (a) Temperature of Melting and (b) Melting Enthalpy (Bee , et al., 2018)

Differential Scanning Calorimetry (DSC) test is conducted to measure melting temperature, and melting enthalpy of polymer. The consequence of irradiation on thermal property of polymer composite is as shown in Figure 2.4. Irradiation induces the formation of crosslinking network by attacking the hydroxyl groups, thus amount of hydroxyl groups in PVOH matrix reduces. This leads to weakening of hydrogen bonds and reduction in melting temperature of pristine PVOH. The addition of CS and DAS into polymer matrix also decrease the melting temperature compared to melting temperature of pristine PVOH. The irregularity for corn starch molecule and dialdehyde starch molecule interrupt the chains arrangements inside PVOH matrix and weakened the interaction of polymer blends.

For polymer blends, irradiation from 0 kGy to 20 kGy increases the melting temperature due to the creation of crosslinking network that enlarges the size of PVOH molecules and starch molecules and promotes the inter-molecular interaction in polymeric matrix (Khonakdar, et al., 2006). Further increment from 20 kGy to 30 kGy decreases the melting temperature due to decrement of the available hydroxyl groups. Besides, the availability of free radicals to form crosslinking network has reduced upon higher irradiation dose, resulting smaller molecular size of polymer chain and weaker

inter-molecular bonds in PVOH composite. The weakening action of hydrogen bonding and intermolecular bonding inside polymer matrix decreases the melting temperature. In Figure 2.5 (b), it is obvious that the enthalpies of melting in pristine PVOH and polymer blends have similar trends as in melting temperature of pristine PVOH and polymer blends.

2.9 Scanning Electron Microscopy (SEM)

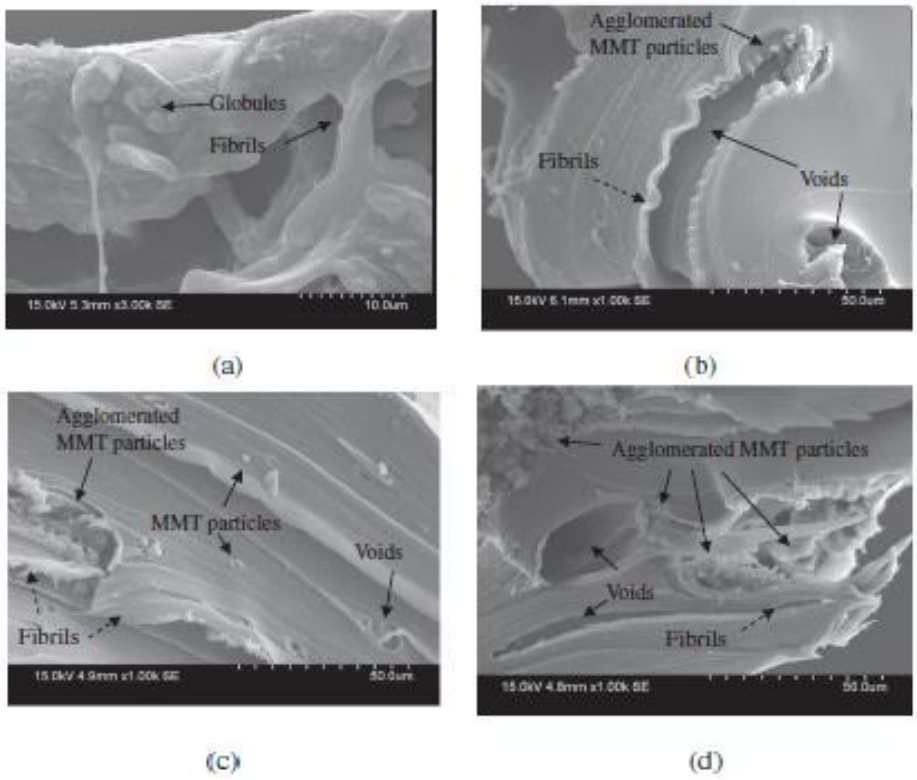

Figure 2.5: SEM Micrograph for Non-Irradiated (a) Pristine Polyvinyl Alcohol and Polyvinyl Alcohol Composites with (b) 0.5 phr MMT, (c) 1.5 phr MMT and (d) 4.5 phr MMT (Bee, et al., 2014)

Scanning Electron Microscopy (SEM) is conducted to determine the morphology of polymer blends. For non-irradiated PVOH as in Figure 2.5, the globules and fibrils are formed owing to the stress applied during tensile test. By increasing the MMT loading level, the presence of flakes (agglomerated particles) increases because inhomogeneous distribution of MMT particles in PVOH matrix will cluster together and develop aggregated particles.

For irradiated pristine polyvinyl alcohol as in Figure 2.6, the fibril width increases and the fibrils amount decreases as increment of irradiation dose from 6 kGy

to 16 kGy. This is attributed to the creation of crosslinking networks in polymer composite that reduces the tearing action of polyvinyl alcohol matrix under straining by increasing the matrix continuity (Gad, 2009). However, further increment to 36 kGy, the fibrils become thinner and higher amount due to chain scission of PVOH matrix.

The Figures 2.7 shows the SEM micrograph of the PE-HAP. The hydroxyapatite particles distribute very poorly on polymer matrix without irradiation. Increasing the absorbed dose up to 150 kGy leads to modification of the polymer structure by reducing the agglomeration effect of HAP particles on polymer matrix.

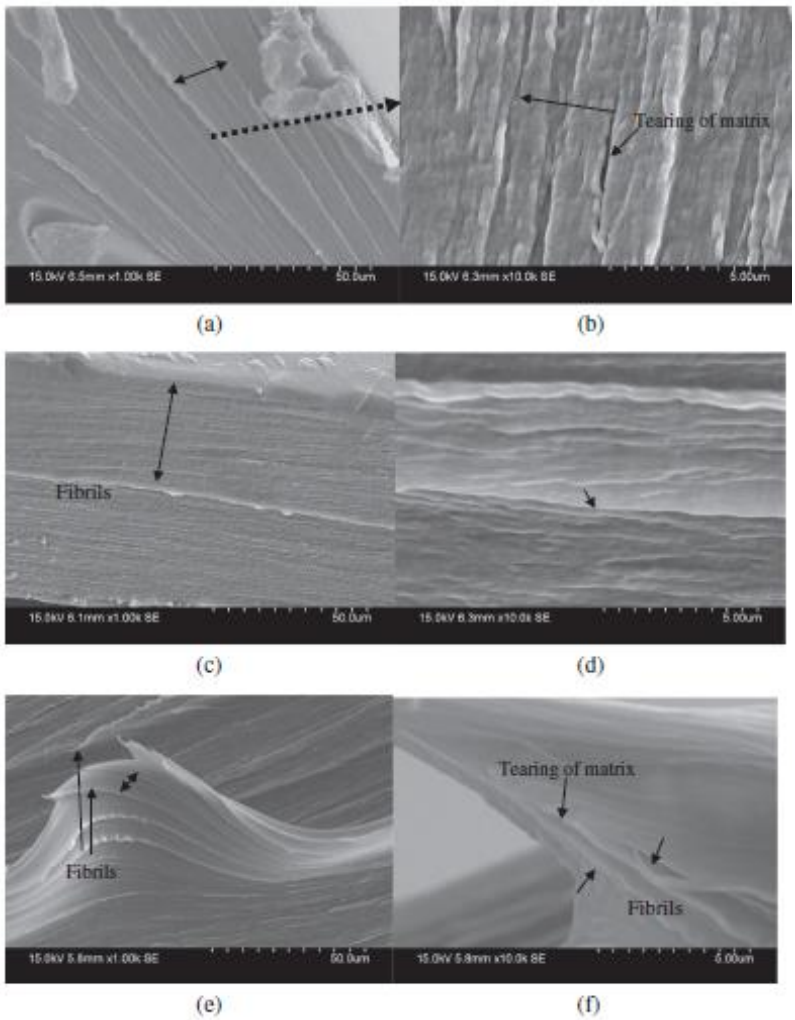

Figure 2.6: SEM Micrograph Pristine Polyvinyl Alcohol under Irradiation Dosages of (a) 6 kGy, (b) 6 kGy, (c) 16 kGy, (d) 16 kGy, (e) 36 kGy and (f) 36 kGy at 10 000 times magnification (Bee, et al., 2014)

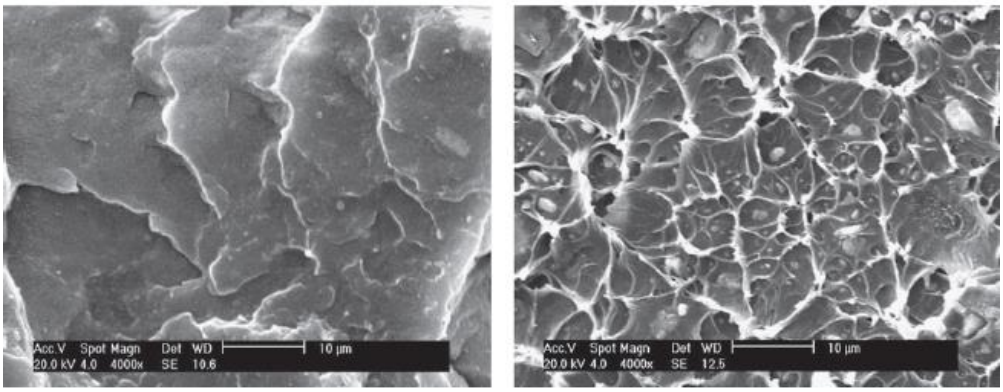

Figure 2.7: SEM Micrograph of the PE-HAP (15%) Composites (a) Non-Irradiated Sample and (b) Irradiated Sample at 150 kGy (Soltani , et al., 2013)

2.10 X-ray Diffraction (XRD)

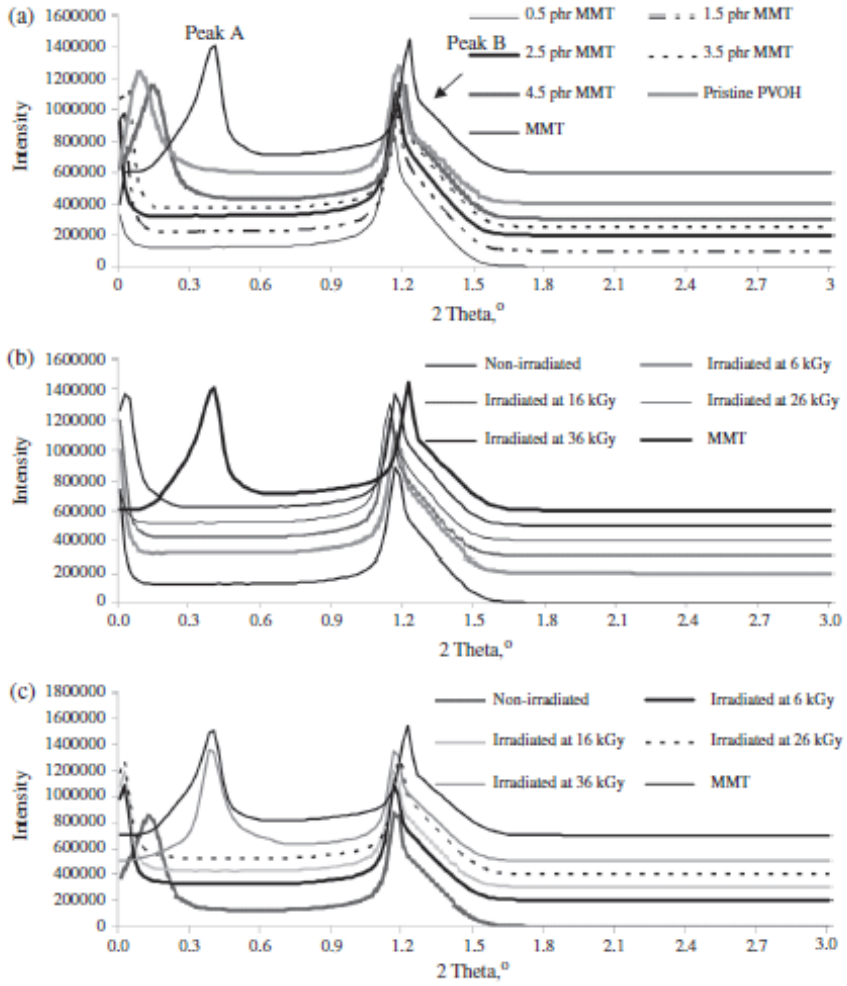

Figure 2.8: XRD Curve ($0° \ll 2\theta \ll 3°$) for (a) Non-Irradiated Polyvinyl Alcohol under different loading of MMT, (b) 0.5 phr MMT in PVOH and (c) 4.5 phr MMT in PVOH (Bee, et al., 2014)

Table 2.2: Crystallinity (%) and Size of Crystallite of Peak C for Polyvinyl Alcohol Composites at different Irradiation Doses (Bee, et al., 2014)

Loading level of MMT, phr	Crystallinity, %				
	0 kGy	6 kGy	16 kGy	26 kGy	36 kGy
0	10.8	10.1	20.1	18.1	10.1
0.5	9.0	11.3	10.4	12.5	18.9
1.5	10.0	15.9	10.0	15.7	16.7
2.5	9.6	15.9	9.7	11.2	9.4
3.5	9.4	9.7	10.7	12.6	10.5
4.5	11.0	16.9	12.2	12.2	6.9
	Crystallite size				
0	43	41	71	40	38
0.5	40	40	41	42	43
1.5	39	85	41	33	41
2.5	43	66	43	43	37
3.5	43	38	39	39	40
4.5	39	78.	40	41	38

X-ray Diffraction (XRD) is used to study the crystallinity and dispersion of fillers on polymer matrix. Figure 2.8 shows the XRD curves of non-irradiated and irradiated PVOH under different loading of MMT. In Figure 2.8 (a), the peak A and peak B of PVOH-MMT composites shifted to lower 2θ as compared to both peaks of pristine montmorillonite. This shows that the polyvinyl alcohol matrix intercalated productively into inter-layer gallery of montmorillonite particles (Yang, et al., 2011). Besides, the d-spacing values of peak B of composite increase comparing to the peak B of pristine MMT owing to the effective scattering of polyvinyl alcohol matrix into the MMT that increases the distance between inter-layers of MMT particles. However, increasing in MMT loading reduces the d-spacing value and interchain separation. This is because increasing of MMT loading promotes agglomeration, hence slightly decreases the amount of effective intercalated MMT particles within PVOH matrix (Bee, et al., 2013).

In Figure 2.8 (b) and Figure 2.8 (c), the peak B of irradiated composite slightly shifts to lower 2θ comparing to the non-irradiated polymer composite. Furthermore, the increment of irradiation dosage from 0 kGy to 26 kGy increases the d-spacing values and interchain separation. This is due to cross-linking network that could enhance the distribution of MMT particles in PVOH matrix. However, further increasing of irradiation dose shifts the peak B to higher 2θ value and causes reduction

in d-spacing and interchain separation. This is so because irradiation does not enhance the scattering process of montmorillonite particle in polymer matrix.

The presence of broad peak C is owing to the non-homogeneous distribution of MMT. The broadening effect on peak C of composites is more obvious than pristine PVOH because crystalline structure in PVOH matrix fractures as 0.5 phr MMT is introduced into polyvinyl alcohol matrix. Table 2.2 illustrates the crystallinity and crystallite size of PVOH at different MMT loading and different irradiation doses. The crystallinity decreases when 0.5 phr MMT is introduced into polyvinyl alcohol matrix because MMT could slightly disrupt the crystallite structure of matrix. As the MMT loading increases up to 4.5 phr, crystallinity increases due to poor distribution of MMT promotes the agglomeration effect. The 4.5 phr composite has the highest crystallinity as the peak A of 4.5 phr composite is sharper than peak A of pristine polyvinyl alcohol.

The crystallinity of pristine polyvinyl alcohol showed a minimal decrement when it is irradiated to 6 kGy based on the higher broadening outcome on width of peak C which proves the rupture of crystallite structure of peak C. The increase in irradiation doses from 6 to 16 kGy increases the crystallinity of pristine polyvinyl alcohol as the appearance of 3 new peaks (peak D, peak E and peak F) on XRD pattern curve shows the creation of three new crystalline structures in pristine polyvinyl alcohol. Electron beam irradiation of 16 kGy changes the chains arrangement of matrix into highly ordered crystal structures. However, the increase irradiation amount from 16 to 26 kGy reduces the crystallinity of pristine polyvinyl alcohol as the peak intensities of peaks D, E, F, and G of 26 kGy irradiated pristine polyvinyl alcohol is decreased dramatically. The highly ordered crystalline structure in pristine PVOH ruptures with further increasing in irradiation amount of 26 kGy. For the irradiation dosage increases up to 36 kGy, the crystallinity of pristine PVOH has reduced as the peaks D, E, F, and G are vanished from XRD pattern. The significant decrement in crystallinity of polyvinyl alcohol composite is chiefly accredited to the destruction of high ordered crystal structure of polymer by chain scission.

2.11 Fourier Transform Infrared (FTIR)

FTIR spectrum of HAP, HDPE, and polymer composite is shown in Figure 2.9. Vibration of the hydroxyl group is observed at about (3575 cm^{-1}). Vibration of phosphate groups is observed at 1036 cm^{-1}, 605 cm^{-1}, 568 $cm^{-1}$and 467 cm^{-1}. Carbonate groups vibration can be differentiated at 873 cm^{-1}, 1417 $cm^{-1}$and 1468 cm^{-1}. It can be

concluded that the obtained sample is carbonate hydroxyapatite. The peaks of HDPE are at 720 cm^{-1} and 1465 cm^{-1}, relating to vibrational of carbon-hydrogen. The composite spectrum indicates the main bands in HDPE and HAP components closely at the same wavelengths. Thus, the little shifts in various functional group wavelengths in the HDPE-HAP composite results in a physical interaction between HAP and HDPE.

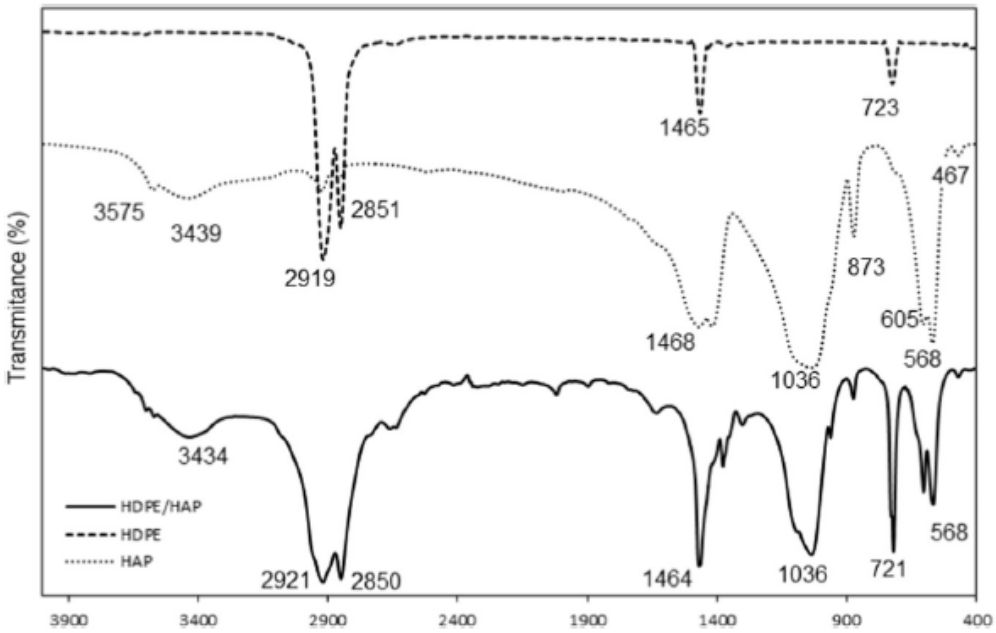

Figure 2.9: FTIR Spectrum of the HAP, HDPE, and HDPE-HAP Nano-Composites (Mohammadi, et al., 2017)

2.12 Thermogravimetric Analysis (TGA)

In Table 2.3, it shows the onset temperature, final temperature, and maximum peak temperature of decomposition for pristine LDPE and LDPE composite. The introduction of MWCNT dramatically improves the thermal stability of LDPE-MWCNT composite. By increasing MWCNT loading, the thermal stability also has been improved. This is due to the hindering action of MWCNT on the diffusion of volatile material (Motaung, et al., 2012) and the formation of stable free radicals (Wang, et al., 2005). The electron beam irradiation decreases thermal stability of the irradiated LDPE-MWCNT composite comparing to the un-irradiated sample due to the destruction of LDPE matrix and MWCNT.

Table 2.3: T_o, T_f and T_p of LDPE and LDPE-MWCNT Composites (Yang, et al., 2015)

Samples	LDPE	Unirradiated samples			LDPE	Irradiated samples		
		LDPE/2% MWCNTs	LDPE/4% MWCNTs	LDPE/8% MWCNTs		LDPE/2% MWCNTs	LDPE/4% MWCNTs	LDPE/8% MWCNTs
T_o (°C)	386 ± 5	419 ± 5	426 ± 5	437 ± 5	366 ± 5	394 ± 5	405 ± 5	415 ± 5
T_f (°C)	485 ± 5	514 ± 5	523 ± 5	538 ± 5	460 ± 5	503 ± 5	512 ± 5	524 ± 5
T_p (°C)	450 ± 5	479 ± 5	483 ± 5	490 ± 5	424 ± 5	470 ± 5	476 ± 5	483 ± 5

CHAPTER 3

METHODOLOGY AND WORK PLAN

3.1 Materials

Fully hydrolysed polyvinyl alcohol is produced by Denki Kagaku Kougyo Kabushiki Kaisya (DENKI) and functioned as polymer base in this project. The hydrolysis of the Denka Poval, K-17C graded PVOH is 87-89 mol%. The viscosity of PVOH is 45-55 mPa.s. Multi-wall carbon nanotube (MWCNT) with diameter of 50nm is manufactured by Ant Spirits Sdn. Bhd. Hard clam shells (Mercenaria Mercenaria) were collected from Kuala Selangor district in Selangor state.

3.2 Fomulation

Table 3.2 shows the formulation composition needed in casting samples. The amount of polyvinyl alcohol used in casting was fixed at 100 phr with different amount of hydroxyapatite and carbon nanotube. Every sample has its abbreviation name as in Table 3.1.

P _ _

Table 3.1: Abbreviation of Sample

Letter	**Stands for**
P	Polymer base
Second letter	CNT amount (phr)
Third letter	HAP amount (phr)

Table 3.2: Composition of PVOH-HAP-CNT in Casting Samples

Sample	PVOH (phr)	CNT (phr)	HAP (phr)	MWR (W)
P11-0	100	1	0.1	0
P15-0	100	1	0.5	0
P21-0	100	2	0.1	0
P25-0	100	2	0.5	0
P11-150	100	1	0.1	150
P15-150	100	1	0.5	150
P21-150	100	2	0.1	150
P25-150	100	2	0.5	150

3.3 Sample Preparation

The hard clams were collected and washed with brush to remove the impurities. The hard clams were later bathed in hot water for 30 minutes. After that, the clams were calcined at temperature of 900 ℃ for two hours in furnace.

The PVOH-HAP-CNT samples were prepared using solution casting method. Initially, the PVOH resin was bathed in distilled water under a water bath of 97 ℃ with tolerance of 2 ℃ for 30 minutes. A stirrer with rotating velocity of 350 rpm was functioned to agitate the mixture of water and polyvinyl alcohol up to the time when all PVOH resin diffused in distilled water. Then, various amount of HAP and CNT were added into PVOH solution as shown in Table 3.1 and agitation was carried out again at the same condition. The mixture solution was casted onto a 6 cm diameter petri dish with approximately 1 mm of thickness. After that, the casted samples were dried inside vacuum oven at 65 ℃ until it reached a constant weight. The dried samples were removed from the dish and sealed in plastic bags at room temperature of 25 ℃ and relative humidity of 65 %.

The casted samples undergone microwave radiation at power 150 W for 10 minutes using microwave oven. In the instrument, irradiation voltage, current and energy were set at 15 kV, 1 mA, and 1 MeV respectively.

3.4 Characterization Test

3.4.1 Tensile Test

Tensile test was conducted using Tinius Olsen H10KS Tensile Microtester. The non-irradiated samples and irradiated samples were cut into rectangular form in accordance to ASTM D882. The samples were situated at the clench of the instrument and aligned in the long axis of the respective specimen.

3.4.2 Differential Scanning Calorimetry (DSC)

Differential scanning calorimetry test was perfomed with the use of Mettler Toledo DSC823 Differential Scanning Calorimeter. The samples with weight of 2-5 mg were determined and loaded into crucible. The sample was then heated to 250 ℃ at heating rate of 20 ℃/min using inert nitrogen gas purge rate of 20ml/min.

3.4.3 Scanning Electron Microscopy (SEM)

Scanning electron microscopy analysis was carried out with the use of Hitachi S-3400N SEM. The samples were cut into small size before mounting with copper stub with the fracture surface positioning upwards. The mounted samples was then covered with a layer of palladium and gold with the use of EMITECH SC7260 Sputter Coater before scanning under an electron beam voltage of 15 kV.

3.4.4 X-ray Diffraction (XRD)

The X-ray diffraction analysis was performed with the use of X-ray Diffraction Shimadzu XRD 6000 diffractometer. The samples were scanned in a range of $5° \ll 2\theta \ll 40°$ in scanning speed of 1.0 °/min. The crystallite size (L) was calculated using Scherrer equation, d-spacing (d) was calculated using Bragg's equation, and interchain separation (R) was determined using Klug and Alexander equation.

$$L = \frac{K\lambda}{\beta cos\theta} \tag{3-1}$$

$$d = \frac{\lambda}{2sin\theta} \tag{3-2}$$

$$R = \frac{5\lambda}{8sin\theta} \tag{3-3}$$

where

K = Scherrer constant (generally the value is 0.9)

β = full width at half maximum (FWHM) of deflection peak

λ = 1.542Å

θ = Bragg angle in radians

3.4.5 Fourier Transform Infrared (FTIR)

Fourier transform infrared analysis was carried out with the use of FTIR machine of ThermoScientific Nicolet iS10 under spectrum from 4000 to 400 cm^{-1}. The samples were placed on the sample holder before scanning.

3.4.6 Thermogravimetric Analysis (TGA)

Thermogravimetric Analysis was performed using thermogravimetric analyser. The samples were run at a heating rate of 20 ℃/min using inert nitrogen gas purge rate of 20 ml/min.

CHAPTER 4

RESULTS AND DISCUSSIONS

4.1 Energy Dispersive X-Ray Spectroscopy (EDX)

Energy dispersive X-ray spectroscopy was carried out for calcined HAP powder to identify the elements present in powder after calcination. The result of EDX analysis had shown in Figure 4.1. Calcium, phosphor, oxygen and hydrogen elements presents in hydroxyapatite (HAP), $Ca_{10}(PO_4)_6(OH)_2$. As seen, oxygen should occupy largest percentage in constitution of this components, followed by calcium, phosphor, and hydrogen. The result in Figure 4.1 shows that oxygen had average atomic percentage of 73.63%; calcium had average atomic percentage of 26.07%; and phosphor had average atomic percentage of 0.30%. The result is consistent with the theoretical amount where oxygen has highest atomic percentage, followed by calcium and phosphor.

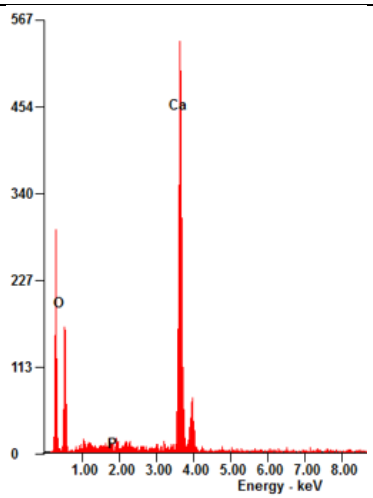

Element	Wt%	At%
O	51.13	72.34
P	00.42	00.30
Ca	48.45	27.36

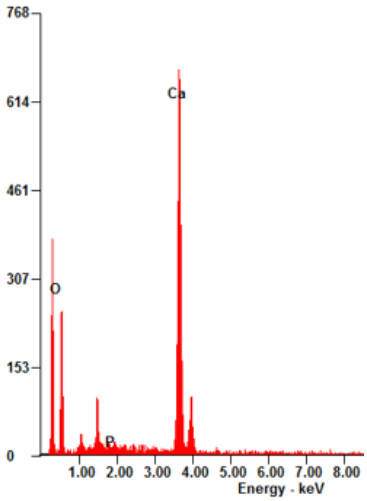

Element	Wt%	At%
O	54.04	74.6
P	0.44	0.32
Ca	45.52	25.08

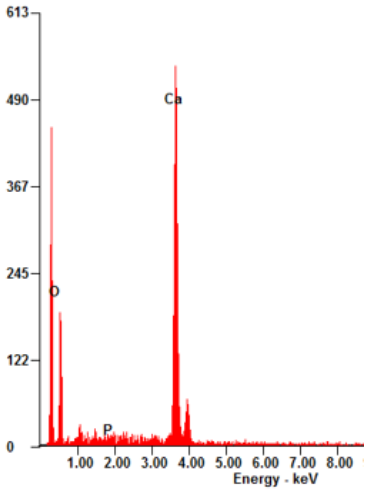

Element	Wt%	At%
O	53.18	73.95
P	0.38	0.27
Ca	46.44	25.78

Average

Element	Wt%	At%
O	52.78	73.63
P	0.41	0.30
Ca	46.80	26.07

Figure 4.1: EDX Analysis on HAP Powder

4.2 Tensile Test

4.2.1 Tensile Strength

Figure 4.2 shows the tensile strength of PVOH nanocomposites added with different loading level of CNT and HAP when subjected to various microwave radiation power.

For PVOH-1 phr CNT non-radiated and radiated polymer nanocomposites, increment of HAP from 0.1 phr to 0.5 phr had decreased the tensile strength of PVOH nanocomposites. This might be due to the presence of low amount of CNT particles that could weaken the interaction effect between PVOH matrix and HAP particles at higher loading level and thus causing the HAP particles to agglomerate into larger particles with higher size irregularity. The presence of HAP particles with irregularity in size and shape could further reduce the interfacial adhesion effect between the PVOH matrix and HAP particles and cause the agglomerated particles to act as stress concentration point during straining, thus leads to the reduction of tensile strength (Zaaba, et al., 2016). In contrast, for PVOH-2 phr CNT non-radiated and radiated polymer nanocomposites, the increment of HAP loading level from 0.1 phr to 0.5 phr was found to marginally increase the tensile strength of PVOH nanocomposites. This might be attributed to the effective interlocking effect of CNT particles at higher loading level that could induce the interaction effect between HAP particles and PVOH matrix and reduce the agglomeration of HAP particles in PVOH matrix. The improvement of the interfacial adhesion between HAP particles and PVOH matrix was mainly attributed to the presence of hydroxyl groups on HAP particles and PVOH matrix which induced the hydrogen bonding between the hydroxyl group on HAP particles and PVOH matrix. The increment in the amount of hydroxyl groups increased the creation of hydrogen bond and therefore enhanced the tensile strength (Zaaba, et al., 2016).

By referring to Figure 4.2, the application of microwave radiation had increased the tensile strength of PVOH-1 phr CNT-HAP polymer nanocomposites because of formation of crosslinked network induced by microwave radiation. The dominance of crosslinking formation instead of chain scissioning might be promoted by low loading of CNT. The crosslinking network able to withstand straining force, therefore enhanced the tensile strength. The application of microwave radiation slightly increased the tensile strength of PVOH-2 phr CNT-0.1 phr HAP polymer nanocomposites. However, application of microwave radiation slightly decreased the

tensile strength of PVOH-2 phr CNT-0.5 phr HAP polymer nanocomposites as a result of the destruction of polyvinyl alcohol structure that was attacked by excessive free radicals. Besides, high loading level of both fillers might also generate agglomeration that acts as stress concentrator and cause reduction of tensile strength. This case is similar to the research conducted by Qu, Zhuo, Wang, Wu, & Cheng (2018) where tensile strength increased with microwave radiation, and then decreased with further increase in radiation.

As CNT increased from 1 phr to 2 phr, it can be observed that tensile strength of PVOH-0.1 phr HAP non-radiated and radiated polymer nanocomposites had decreased. This is attributed to the hydrophobic behavior of CNT that were poorly scattered on hydrophilic PVOH resulted in the formation of CNT agglomerated particles in PVOH matrix. The agglomerated CNT particles were poorly interfacial adhered with PVOH matrix and caused them to act as stress concentration point subjecting to straining. Subsequently, the tensile strength of HAP-PVOH nanocomposites reduced with increasing of CNT loading level (Liu, et al., 2014). On the other hand, tensile strength of PVOH-0.5 phr HAP non-radiated and radiated polymer nanocomposites increased if CNT increased from 1 phr to 2 phr. By increasing HAP loading, the amount of hydroxyl groups available to form hydrogen bond increased (Zaaba, et al., 2016). This had increased the formation of hydrogen bond, improved the interaction of CNT and PVOH, and thus reduced the agglomeration effect as CNT increased from 1 phr to 2 phr, thus causing the increment of tensile strength.

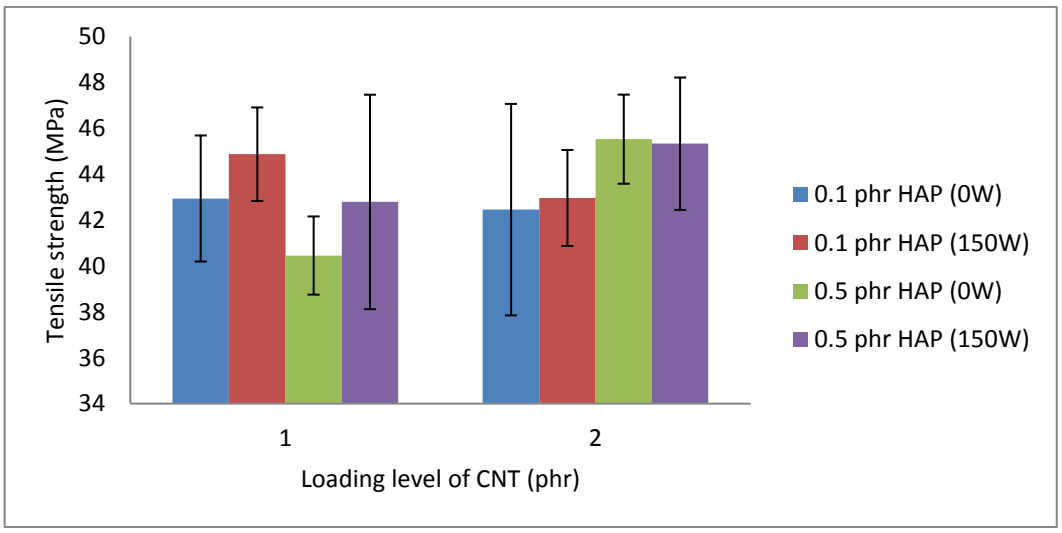

Figure 4.2: Effect of Increasing CNT Loading Level on Tensile Strength

4.2.2 Young's Modulus

Figure 4.3 shows the Young's modulus of PVOH nanocomposites added with different loading of CNT and HAP when subjected to various microwave radiation power.

For PVOH-CNT non-radiated and radiated polymer nanocomposites, increment of HAP from 0.1 phr to 0.5 phr had decreased the Young's modulus. This is due to the weak adhesion between HAP particles and PVOH matrix. The poor adhesion performance produced a weak interfacial zone in which bond was likely to disintegrate. This subsequently reduced the rigidity of polymer blends and decreased the Young's modulus. It is proven by a research which claimed that poor adhesion generated weak interface zone, hence brought about the destruction of bond and frictional pull out (Yao, et al., 2013).

By referring to Figure 4.3, the application of microwave radiation had increased the Young's modulus of PVOH-1 phr CNT-HAP polymer nanocomposites due to formation of crosslinking. However, application of microwave radiation slightly increased the Young's modulus of PVOH-2 phr CNT-HAP polymer nanocomposites. The little increment might be caused by the high loading of CNT that motivated the formation of agglomerated particles. The agglomeration slightly reduced the increment of Young's modulus for PVOH-2 phr CNT-HAP polymer nanocomposites. This trend is confirmed by a study which declared that microwave radiation greatly enhanced the Young's modulus of buckypapers/polyethylene (BPs-n/PE) composites (Qu, et al., 2018).

As CNT increased from 1 phr to 2 phr, it can be seen that Young's modulus of all PVOH-HAP non-radiated and radiated polymer nanocomposites had increased. It is known that incorporation of filler promotes strong reinforcing action (Katerinopoulou, et al., 2014). CNT can act as reinforcing agent that induces high rigidity on polymer blends, then increases the Young's modulus of polymer nanocomposites.

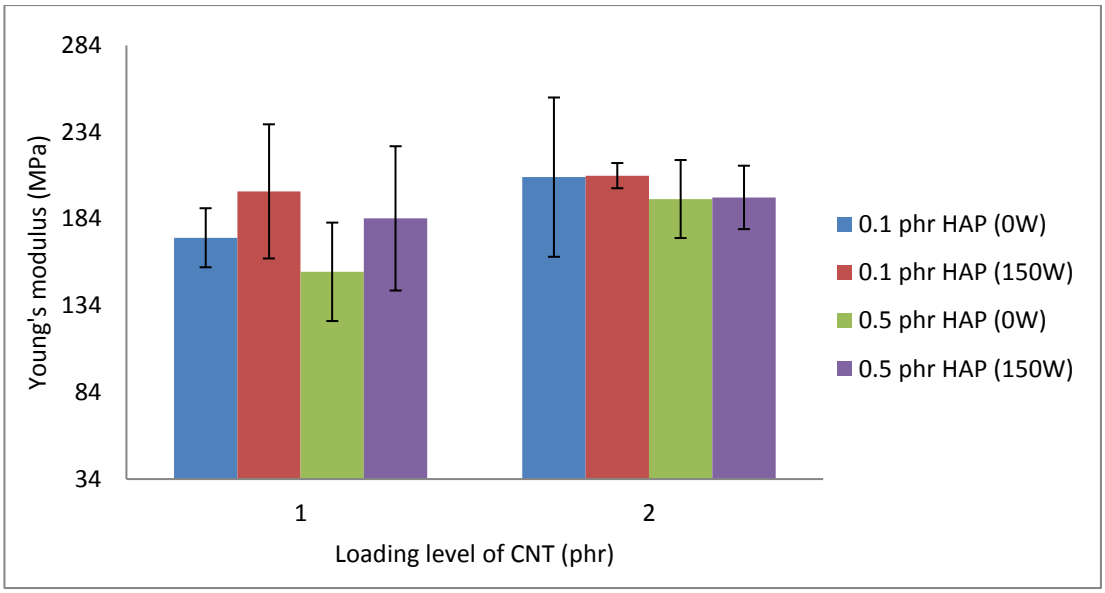

Figure 4.3: Effect of Increasing CNT Loading Level on Young's Modulus

4.2.3 Elongation at Break

Figure 4.4 shows the Young's modulus of PVOH nanocomposites added with different loading level of CNT and HAP when subjected to various microwave radiation power.

For PVOH-1 phr CNT non-radiated and radiated polymer nanocomposites, increment of HAP from 0.1 phr to 0.5 phr had decreased the elongation at break. The interaction of HAP particles and PVOH matrix might be worsen by the 1 phr CNT. Thus, poor dispersion of HAP particles on PVOH blends reduced the chain sliding ability and so reduced the elongation at break. From a study reported by Katerinopoulou, et al., (2014) concluded that elongation at break decreased with increment in NaMMT content due to the prevention of chain sliding against each other. For PVOH-2 phr CNT non-radiated polymer nanocomposites, increment of HAP from 0.1 phr to 0.5 phr slightly increased the elongation at break. This is because sufficient amount of CNT was incorporated that enhanced the interaction of HAP and polymer matrix, hence promoted sliding of chains and improved the elongation at break. However, for PVOH-2 phr CNT radiated polymer nanocomposites, increment of HAP from 0.1 phr to 0.5 phr had decreased the elongation at break. . This is due to high loading level of CNT that enhanced the interaction of HAP particles and polymer matrix, therefore reducing the chain sliding ability. Besides, microwave radiation at 0.5 phr HAP induced formation of crosslinking that reduced the ability of chain to slide. Therefore, the elongation at break decreased as compared to PVOH-2 phr CNT non-radiated polymer nanocomposites. Furthermore, the reinforcing filler (HAP)

strengthened the polymer blends and reduced the polymer ductility, this caused the reduction in elongation at break (Zaaba, et al., 2016).

By referring to Figure 4.4, the application of microwave radiation on PVOH-CNT-HAP polymer nanocomposites had increased the elongation at break. This might be attributed to the crosslinking network induced by radiation that allowed the entanglement of polymer to increase. As polymer is highly entangled, it enable the polymer to be elongated longer under stress. From Qu, Zhuo, Wang, Wu, & Cheng (2018), mechanical properties of BPs/PE composites can be enhanced by microwave radiation. The results show that microwave radiation improved tensile strength, Young's modulus, and elongation of PVOH blends. However, application of microwave radiation on PVOH-1 phr CNT-0.5 phr HAP polymer nanocomposites only slightly increased the elongation at break. This was being explained previously at which elongation at break reduced when HAP loading increased.

As CNT increased from 1 phr to 2 phr, it can be seen that elongation at break of all PVOH-HAP non-radiated and radiated polymer nanocomposites had decreased. This is contributed to the agglomeration of CNT on PVOH blends that weaken the reinforcing action of CNT. Agglomeration of CNT filler on polymer matrix inhibited the uniform flow of polymer nanocomposites upon elongation (Bee, et al., 2014). Thus at high loading level of CNT, CNT particles dispersed unevenly and formed clusters, hence brought about decrement in elongation at break. Another research conducted by Zaaba, Ismail, & Mariatti (2016) stated that the incorporation of filler into the recycled polypropylene-peanut shell powder (RPP/PSP) composite reduced the toughness, resulting into decrement of elongation at break. Addition of CNT loading level might reduce the toughness of polymer blends, causing reduction of the ability to deform before fracture and leads to decrease of elongation at break.

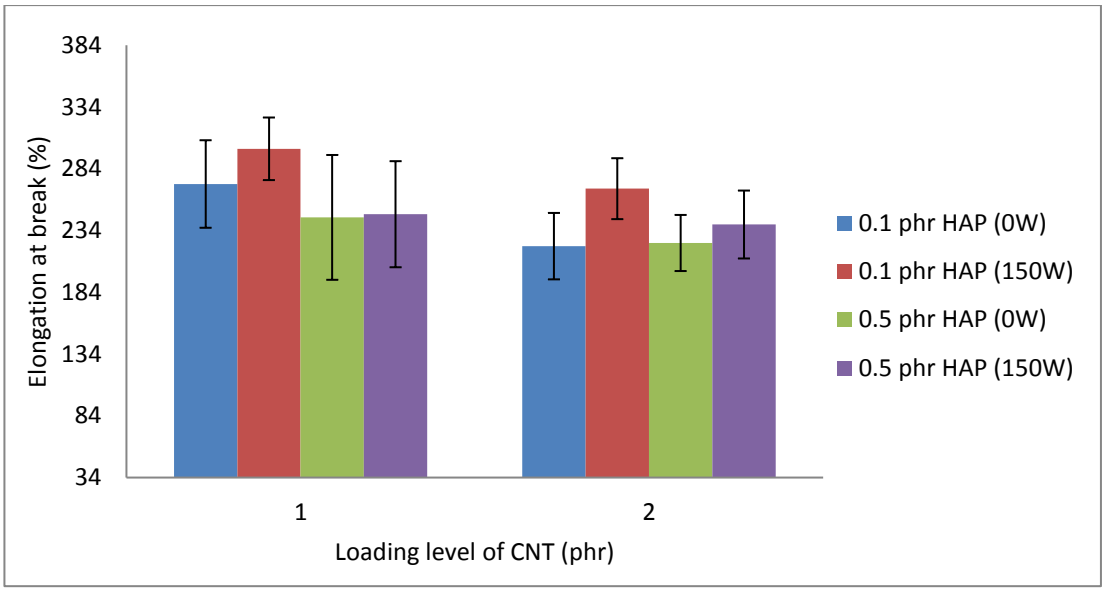

Figure 4.4: Effect of Increasing CNT Loading Level on Elongation at Break

4.3 Differential Scanning Calorimetry (DSC)

Figure 4.5 and Figure 4.6 show the DSC curves for non-radiated PVOH blends and 150 W radiated PVOH blends. Figure 4.7 and Figure 4.8 show the melting temperature and enthalpy pf melting of PVOH nanocomposites added with different loading level of CNT and HAP respectively when subjected to various microwave radiation power.

4.3.1 Melting Temperature

For PVOH-1 phr CNT radiated polymer nanocomposites, increment of HAP from 0.1 phr to 0.5 phr had decreased the melting temperature of PVOH nanocomposites. This is due to low loading level of CNT that interrupted the interaction of HAP particles and polymer matrix. Thus, increasing the amount of HAP at low loading level of CNT promoted agglomeration and subsequently formed large particles with higher size irregularity. This irregularity of HAP particles disrupted the chain arrangement of polymer matrix. Besides, high loading of HAP might induce the crosslinking that attacks hydroxyl group and thus reducing the amount of hydroxyl groups. This leads to weakening of hydrogen bonds and reduction in melting temperature (Bee, et al., 2014). Therefore, the melting temperature of PVOH-1 phr CNT radiated polymer nanocomposites reduced in virtue of these two factors. In contrast, for PVOH-1 phr CNT non-radiated polymer nanocomposites and PVOH-2 phr CNT non-radiated and radiated polymer nanocomposites, the increment of HAP loading level from 0.1 phr to 0.5 phr had increased the melting temperature of PVOH nanocomposites. This is

attributed to the rigidity of the reinforcing filler (HAP) that enhanced the structure of polymer blends (Soltani , et al., 2013). In addition, the hydrogen bonds in HAP inhibited the mobility of chain, thus generated higher rigidity and strength for polymer nanocomposite (Rwei & Huang, 2012). The high rigidity proposed by HAP filler effectively improved the melting temperature of PVOH blends.

The application of microwave radiation had decreased the melting temperature of PVOH-1 phr CNT-HAP polymer nanocomposites. This is because low loading of CNT absorbed heat during microwave radiation. The absorbed heat energy weaken the interaction of CNT and polymer matrix by breaking the chemical bonds (Qu, et al., 2018). Furthermore, low loading of CNT promoted crosslinking that attacked hydroxyl group and reduced the amount of hydrogen bonds, causing decrement in melting temperature. As a consequence, the melting temperature decreased when microwave radiation was applied. However, the application of microwave radiation had increased the melting temperature of other composition of PVOH-2 phr CNT-HAP polymer nanocomposites. This is because 2 phr CNT induced chain scissioning that reduced the attacking action of free radicals, therefore improved the hydrogen bonds and melting temperature of PVOH-2 phr CNT-HAP polymer nanocomposites.

As CNT increased from 1 phr to 2 phr, melting temperature of PVOH-HAP non-radiated polymer nanocomposites had decreased. This might be owing to the non-homogeneous dispersion of CNT on PVO-HAP polymer blends. On the other hand, melting temperature of PVOH-HAP radiated polymer nanocomposites had increased if CNT increased from 1 phr to 2 phr. The rigidity of CNT particles and microwave radiation increased the melting temperature of polymer blends.

4.3.2 Enthalpy of Melting

For PVOH-1 phr CNT radiated polymer nanocomposites, increment of HAP from 0.1 phr to 0.5 phr had decreased the enthalpy of melting of PVOH nanocomposites. As discussed in melting temperature, the agglomeration due to high loading of HAP and reduction of hydroxyl groups due to crosslinking induced by radiation causing the enthalpy of melting to decrease. In contrast, for PVOH-1 phr CNT non-radiated polymer nanocomposites and PVOH-2 phr CNT non-radiated and radiated polymer nanocomposites, the increment of HAP loading level from 0.1 phr to 0.5 phr had increased the enthalpy of melting of PVOH nanocomposites. This indicates that

crystallinity increased when higher amount of HAP was incorporated on those polymer blends.

The application of microwave radiation had decreased the enthalpy of melting of PVOH-1 phr CNT-0.5 phr HAP polymer nanocomposites. This decrement in enthalpy of melting shows that radiated PVOH-1 phr CNT-0.5 phr HAP polymer nanocomposites had lower crystallinity. However, the application of microwave radiation had increased the enthalpy of melting of other composition of PVOH-CNT-HAP polymer nanocomposites. This is because of the microwave radiation that formed new bonds and improved the crystallinity of polymer blends.

As CNT increased from 1 phr to 2 phr, it can be observed that enthalpy of melting of PVOH-0.1 phr HAP non-radiated polymer nanocomposites had decreased. This was caused by the 0.1 phr HAP that reduced the interaction effect of CNT filler and polymer matrix. As can be seen, the addition of CNT on PVOH-0.1 phr HAP non-radiated polymer nanocomposites disrupted the crystalline structure and decreased the crystallinity. On the other hand, that enthalpy of melting of PVOH-0.5 phr HAP non-radiated polymer nanocomposites and PVOH-HAP radiated polymer nanocomposites had increased if CNT increased from 1 phr to 2 phr. This is due to the reason of stiffening behaviour of CNT that improved the crystallinity of PVOH nanocomposites (Sandler, et al., 2003).

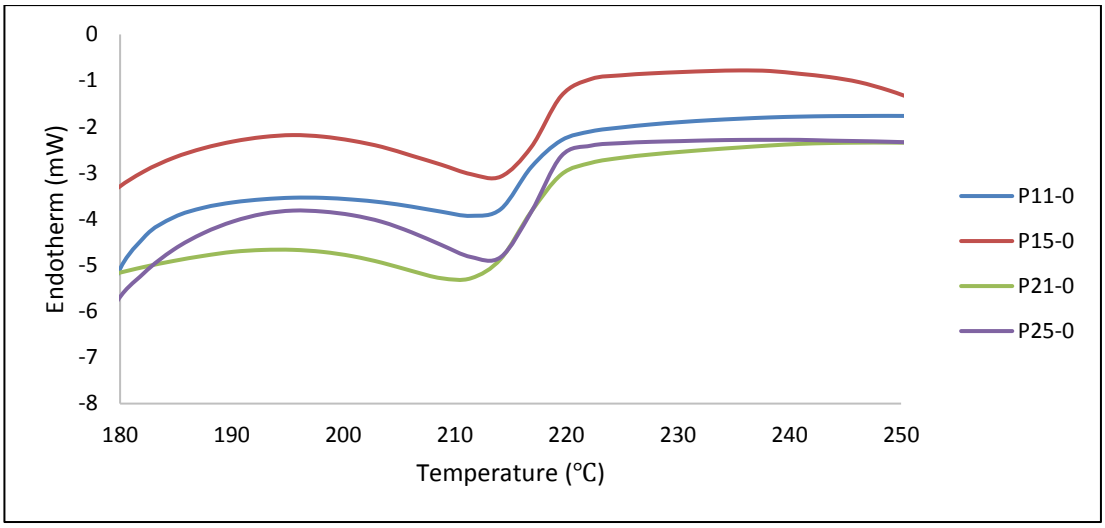

Figure 4.5: DSC Thermogram of Non-Radiated Polymer Composite with Composition of (a) 100phr PVOH-1phr CNT-0.1phr HAP, (b) 100phr PVOH-1phr CNT-0.5phr HAP, (c) 100phr PVOH-2phr CNT-0.1phr HAP, and (d) 100phr PVOH-2phr CNT-0.5phr HAP

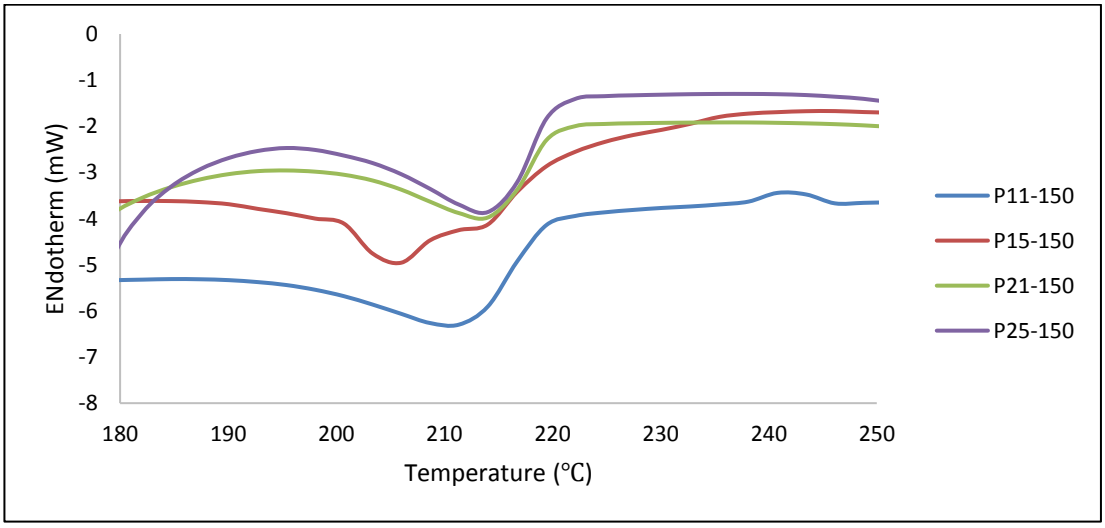

Figure 4.6: DSC Thermogram of 150 W Radiated Polymer Composite with Composition of (a) 100phr PVOH-1phr CNT-0.1phr HAP, (b) 100phr PVOH-1phr CNT-0.5phr HAP, (c) 100phr PVOH-2phr CNT-0.1phr HAP, and (d) 100phr PVOH-2phr CNT-0.5phr HAP

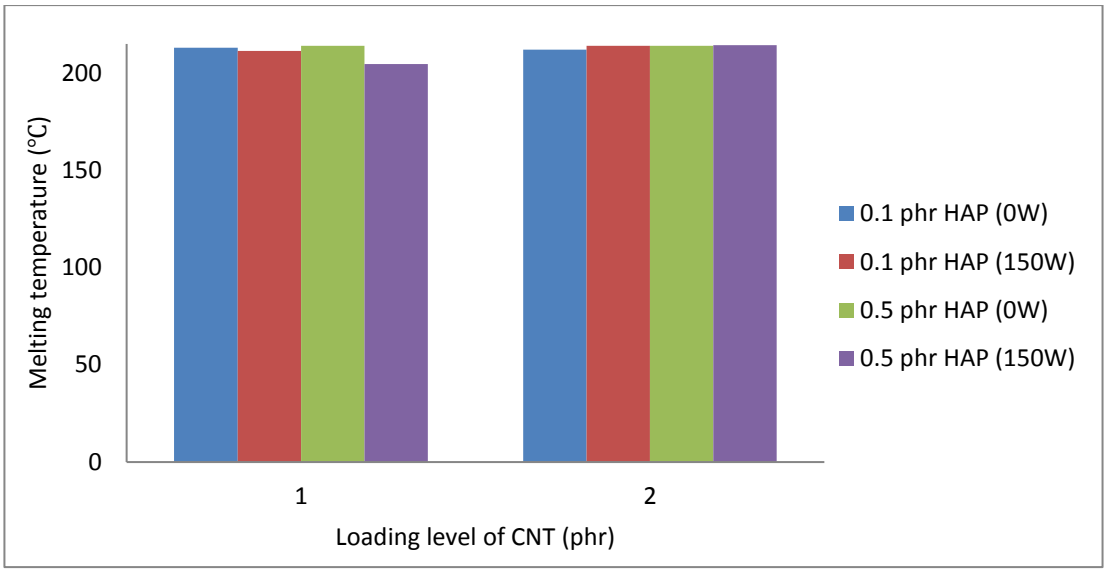

Figure 4.7: Effect of Increasing CNT Loading Level on Melting Temperature

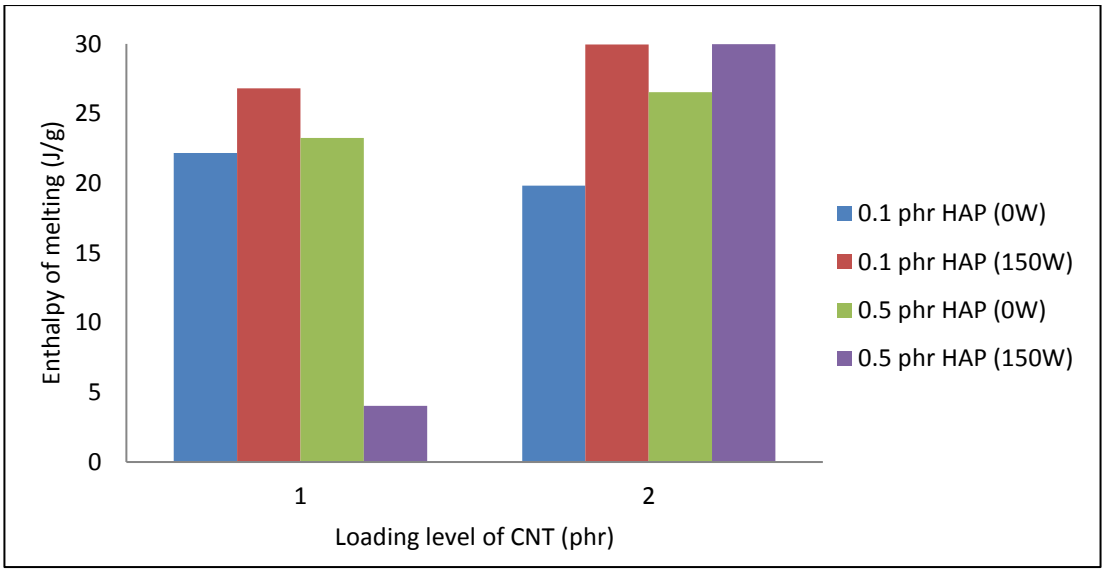

Figure 4.8: Effect of Increasing CNT Loading Level on Enthalpy of Melting

4.4 Scanning Electron Microscopy (SEM)

Figure 4.9 shows the fractured surface morphologies of non-radiated PVOH blends while Figure 4.10 shows the fractured surface morphologies of 150 W radiated PVOH blends.

The presence of flakes is observed in Figure 4.9 (b), (c) and Figure 4.10 (b), (c). The presence of flakes is due to the non-homogenous dispersion of HAP or CNT particles in polymer blends that clustered together to form agglomerated particles. By increasing the loading level of HAP or CNT, the performance of particles dispersion became poorer, this leads to increasing agglomerated particles on polymer matrix, thus

more flakes can be found on higher loading level of HAP or CNT. According to Zaaba, Ismail, & Mariatti (2016), recycled polypropylene/peanut shell powder (RPP/PSP) composite at low loading of filler had rough surface but at high loading of filler had high porosity structure and more agglomeration. As discussed above, the agglomeration effect reduced the tensile strength of polymer composite because agglomerated particles weaken the reinforcing effect of HAP and CNT fillers. A research done by Supri and Lim (2009) claimed that the amount of filler was related to the tendency of brittle cracking. This shows that higher filler loading in polymer composite that promoted agglomeration had lower tensile strength. This can be seen in the tensile test result where 100 phr PVOH-1 phr CNT-0.5 phr HAP sample and 100 phr PVOH-2 phr CNT-0.1 phr HAP sample had relatively lower tensile strength than 100 phr PVOH-1 phr CNT-0.1 phr HAP sample and 100 phr PVOH-2 phr CNT-0.5 phr HAP sample. Increment in filler loading that increases agglomeration effect is destructive to mechanical properties.

The formation of fibrils can be observed in Figure 4.9 and Figure 4.10. Formation of fibrils is due to the stress applied to elongate the PVOH sample when tested by tensile machine. From Figure 4.9 (a), (b), and (c), the width of fibrils is shorter and fibrils amount is higher comparing to Figure 4.10 (a), (b), and (c). This is because 150 W radiation generated crosslinking network that improved the continuity of polymer matrix, and therefore reducing the amount of fibrils. Bee, et al. (2014) stated that radiation promoted formation of crosslinking networks in polymer matrix that able to withstand the tearing effect by external force and increase the matrix continuity of PVOH composite. A similar findings was reported by Soltani , Ziaie , Ghaffari , Afarideh, & Ehsani (2013) whereby the HAP particles had poor interaction with the polymer with no radiation but polymer became stiffer as radiation was applied. This statement can be proven by SEM micrograph below where radiated polymer sample exhibited longer fibrils width and lower fibrils amount. However, 100 phr PVOH-2 phr CNT-0.5 phr HAP sample did not obey the trend. This might be due to the chain scissioning induced by microwave radiation that deteriorates the mechanical properties. Apart from that, it is observed that agglomerated particles in Figure 4.5 was lesser compared to Figure 4.4 because radiation helped minimizing the agglomeration effect of filler by improving intercalation and dispersion of HAP and CNT on polymer composite. As discussed previously, application of microwave radiation enhances mechanical properties of polymer composite. This is contributed to the mechanism of

cross-linking and minimization of agglomerated particles under the application of microwave radiation. This can be seen in the tensile test result where radiated PVOH nanocomposites had higher tensile strength than non-radiated PVOH nanocomposites.

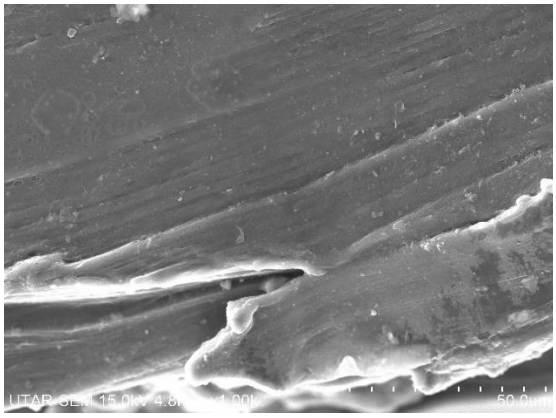

(a) P11-0

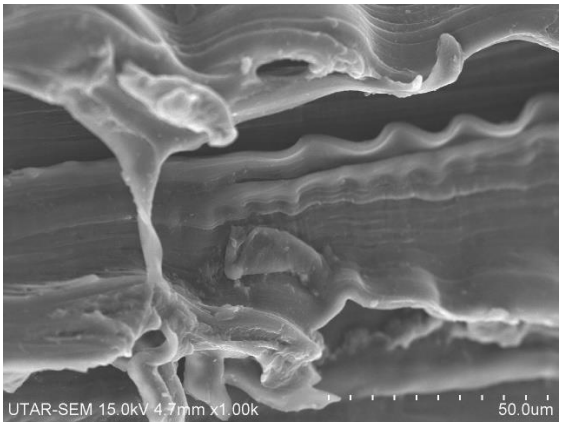

(b) P15-0

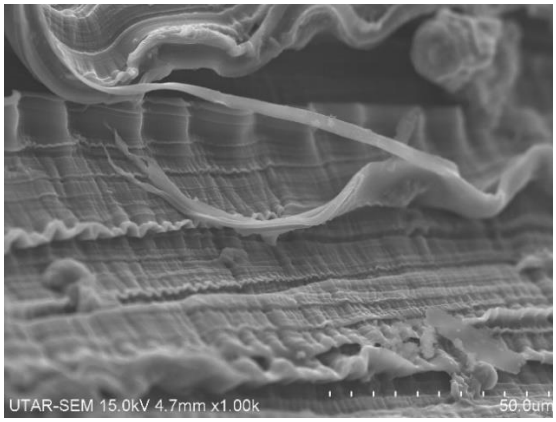

(c) P21-0

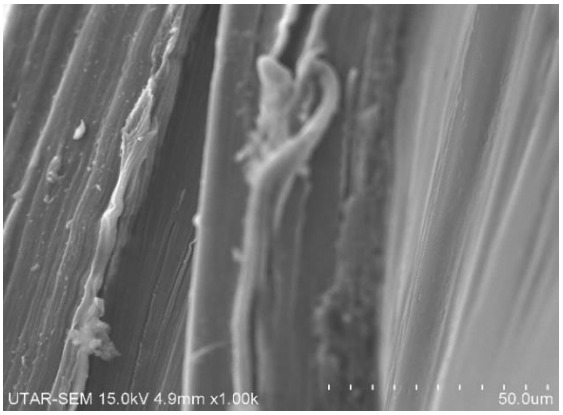

(d) P25-0

Figure 4.9: SEM micrographs of Fractured Surface for Non-Radiated Polymer Composite with Composition of (a) 100 phr PVOH-1 phr CNT-0.1 phr HAP, (b) 100 phr PVOH-1 phr CNT-0.5 phr HAP, (c) 100 phr PVOH-2 phr CNT-0.1 phr HAP, and (d) 100 phr PVOH-2 phr CNT-0.5 phr HAP under magnification of 1000 times

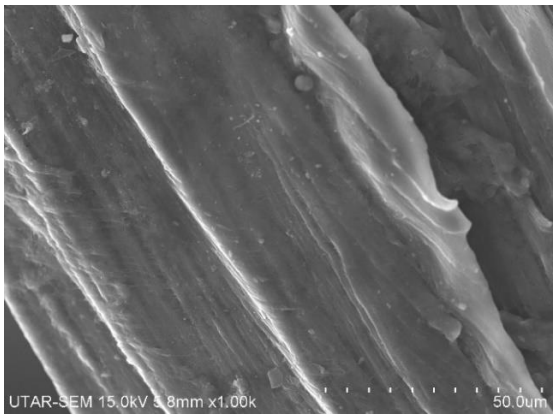

(a) P11-150

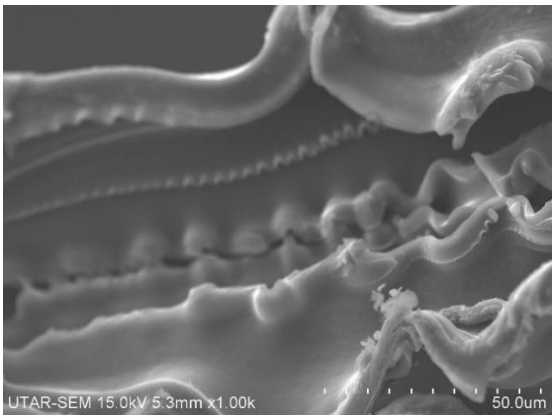

(b) P15-150

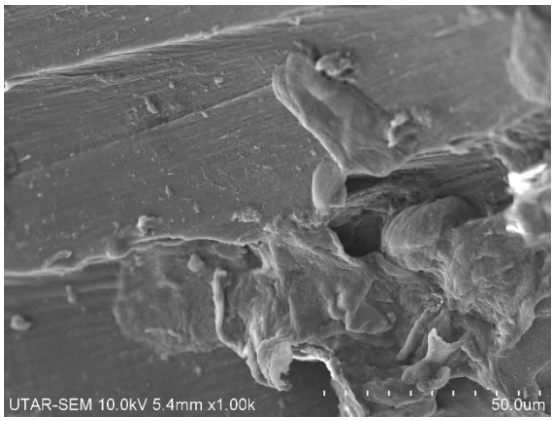

(c) P21-150

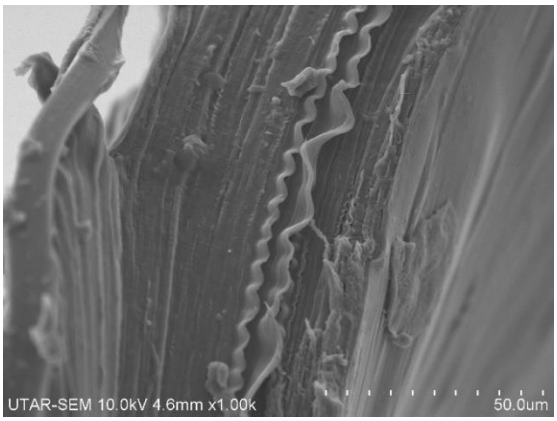

(d) P25-150

Figure 4.10: SEM micrographs of Fractured Surface for 150 W Radiated Polymer Composite with Composition of (a) 100 phr PVOH-1 phr CNT-0.1 phr HAP, (b) 100 phr PVOH-1 phr CNT-0.5 phr HAP, (c) 100 phr PVOH-2 phr CNT-0.1 phr HAP, and (d) 100 phr PVOH-2 phr CNT-0.5 phr HAP under magnification of 1000 times

4.5 X-ray Diffraction (XRD)

Figure 4.11 and Figure 4.12 show the XRD curves for non-radiated PVOH blends and 150 W radiated PVOH blends. Table 4.1 and Table 4.2 illustrate two theta, crystallite size, d-spacing, and interchain separation of deflection peak A and B for non-radiated PVOH blends and 150 W radiated PVOH blends.

4.5.1 Dispersion of CNT on Polymer Composite

Referred to Table 4.1 and Table 4.2, increment of CNT from 1 phr to 2 phr had decreased the d-spacing and interchain separation (peak B) of PVOH-0.1 phr HAP non-radiated and radiated polymer nanocomposites. This illustrates that high loading

level of CNT reduced the effective intercalation of CNT on PVOH-0.1 phr HAP polymer blends. This is due to the reason of agglomeration that happened only at high loading level of filler. Low loading of HAP reduced the interaction between CNT and PVOH, leading to agglomeration as CNT loading level was increased. Agglomeration reduced the effectiveness of intercalation of CNT. Thus, it is concluded that high loading level of CNT induces agglomeration, affects the CNT intercalation action, and consequently reduces the d-spacing and interchain separation of PVOH-0.1 phr HAP non-radiated and radiated polymer nanocomposites (Bee, et al., 2014).

In contrast, increment of CNT from 1 phr to 2 phr had increased the d-spacing and interchain separation (peak B) of PVOH-0.5 phr HAP non-radiated and radiated polymer nanocomposites. This shows that 2 phr CNT improved the intercalation of CNT on PVOH-0.5 phr HAP polymer blends. From that, it is known that 0.5 phr HAP improves the interaction of CNT particles and PVOH matrix. Hence, increasing CNT loading level increased the effective intercalation of CNT on PVOH-0.5 phr HAP polymer blends. The increment and decrement of d-spacing of polymer nanocomposites is consistent with the tensile test results where d-spacing and tensile strength for PVOH-0.1 phr HAP polymer blends reduced but d-spacing and tensile strength for PVOH-0.5 phr HAP polymer blends increased when CNT is increased from 1 phr to 2 phr. This indicates that the d-spacing is directly related to the tensile strength of polymer nanocomposites.

4.5.2 Dispersion of HAP on Polymer Composite

Referred to Table 4.1 and Table 4.2, the d-spacing and interchain separation (peak B) of PVOH-1 phr CNT non-radiated and radiated polymer nanocomposites had decreased as HAP was added from 0.1 phr to 0.5 phr. This is because 1 phr CNT weaken the interaction of HAP particles and PVOH matrix. In consequence, agglomerated particles increased as HAP loading level increased. As discussed above, agglomeration reduces the effectiveness of intercalation. Based on the weakening effect of CNT on interaction between HAP and PVOH, it is said that the high loading level of HAP induces agglomeration, and therefore reduces the d-spacing and interchain separation of PVOH-1 phr CNT polymer nanocomposites.

However, the d-spacing and interchain separation (peak B) of PVOH-2 phr CNT non-radiated and radiated polymer nanocomposites had increased as HAP was added from 0.1 phr to 0.5 phr. This increment shows that that high loading level of

HAP improved the effective intercalation of HAP on PVOH-2 phr CNT polymer blends. It can be observed that 2 phr CNT improved the interaction of HAP particles and PVOH matrix due to the excellent effective locking effect of CNT particles at high loading level. Correspondingly, the increment of HAP loading level increased the d-spacing and interchain separation of PVOH-2 phr CNT polymer nanocomposites. By comparing the effect of addition of CNT and HAP on d-spacing, it is known that the result trends are similar. From that, it can be concluded that the mechanism for addition of both filler on polymer blends are analogous, and this leads to similar trends for d-spacing.

4.5.3 Effect of Microwave Radiation on Dispersion of Filler

As mentioned previously, microwave radiation affected the dispersion of HAP and CNT fillers on polymer nanocomposite. The change in dispersion of both fillers also affected the amount of agglomeration particles on polymer matrix. Referred to Table 4.1 and Table 4.2, the application of microwave radiation had decreased the d-spacing and interchain separation (peak B) of PVOH-1 phr CNT-HAP polymer nanocomposites. It is known that the CNT is excellent microwave absorbents that absorb the heat from microwave radiation (Qu, et al., 2018). Under the application of microwave radiation, the intense heat absorbed by CNT within polymer nanocomposites weaken the intercalation of CNT and HAP particles on polymer matrix, thus reducing the d-spacing and interchain separation of PVOH-1 phr CNT-HAP polymer nanocomposites. Besides, the hydrophobic behaviour of CNT also interfered the dispersion of filler on hydrophilic polymer blends (Liu, et al., 2014).

On the other hand, application of microwave radiation had increased the d-spacing and interchain separation (peak B) of PVOH-2 phr CNT-HAP polymer nanocomposites. CNT is a reinforcing filler that allows the enhancement of interaction of filler towards polymer matrix, but it only applicable when the amount of CNT is sufficient to trigger the reinforcing action (Sandler, et al., 2003). Moreover, microwave radiation which induces formation of cross-linking is able to improve the intercalation effect (Bee, et al., 2014). In short, the high loading of CNT and application of microwave radiation increased d-spacing and interchain separation of PVOH-2 phr CNT-HAP polymer nanocomposites.

4.5.4 Crystallinity

Referred to Table 4.1 and Table 4.2, increment of CNT from 1 phr to 2 phr had decreased the crystallite size (peak A) of PVOH-HAP non-radiated and radiated polymer nanocomposites. Similarly, the crystallite size (peak A) of PVOH-CNT non-radiated and radiated polymer nanocomposites had decreased as HAP was added from 0.1 phr to 0.5 phr. This is contributed to the incorporation of CNT and HAP particles on polymer matrix that disrupted the crystalline structure of PVOH matrix. The orientation of crystalline structure was ruptured when CNT or HAP was added (Bee, et al., 2014). This is observed in Figure 4.11 and Figure 4.12 whereby the broadening effect of peak A had increased upon addition of CNT or HAP fillers. In short, increment of loading level of CNT or HAP reduces the crystallite size and increases the peak broadening effect. This reveals the disruption of crystallite structure when CNT or HAP was incorporated in the polymer matrix.

The application of microwave radiation had decreased the crystallite size (peak A) of PVOH-CNT-HAP polymer nanocomposites. This is due to the breakdown of bond by chain scission that disrupted the structure of highly ordered chains arrangement thus leading to a structure of less ordered chain arrangement (Bee , et al., 2018). This disordered structure reduced the crystallinity of PVOH-CNT-HAP polymer nanocomposites. A findings by Soltani , et al. (2013) stated that radiation prevented the growth of crystal and decreased the amount and size of crystals. The decrement in crystallite size produced a more amorphous nature of polymer nanocomposites which promoted the degradation on polymer film (Somashekarappa, et al., 2013). This can be observed in Figure 4.11 and Figure 4.12 where XRD curves in Figure 4.12 had higher peak broadening than XRD curves in Figure 4.11. The broadening of peak indicates that existence of amorphous state. To be concluded, as crystallite size decreases under radiation, peak broadening becomes more obvious, this shows that more crystallite structure has been destructed to amorphous by the application of microwave radiation.

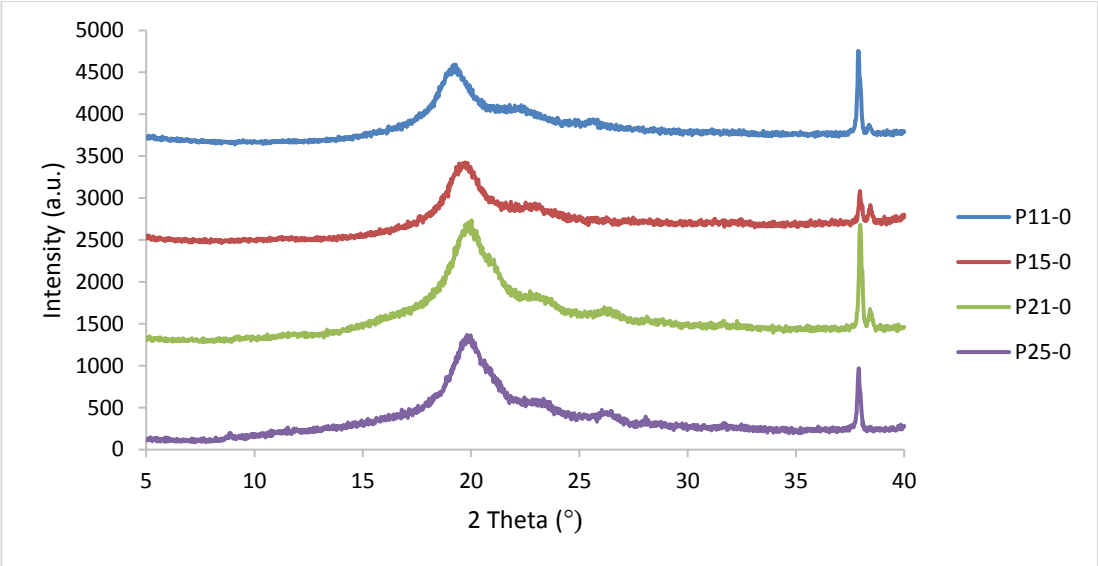

Figure 4.11: XRD Curve for Non-Radiated Polymer Composite with Composition of (a) 100 phr PVOH-1 phr CNT-0.1 phr HAP, (b) 100 phr PVOH-1 phr CNT-0.5 phr HAP, (c) 100 phr PVOH-2 phr CNT-0.1 phr HAP, and (d) 100 phr PVOH-2 phr CNT-0.5 phr HAP

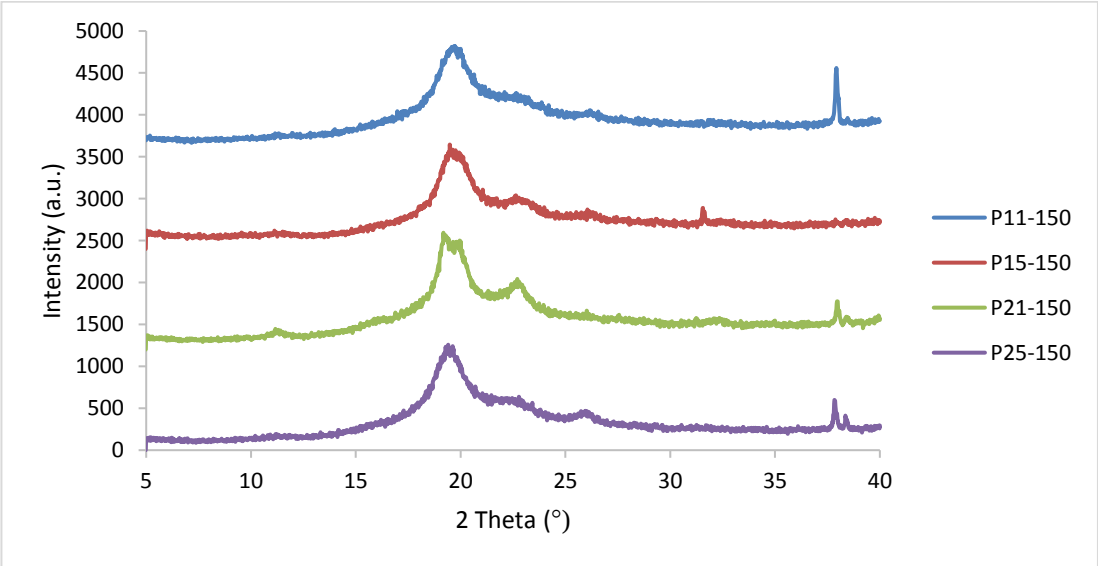

Figure 4.12: XRD Curve for 150 W Radiated Polymer Composite with Composition of (a) 100 phr PVOH-1 phr CNT-0.1 phr HAP, (b) 100 phr PVOH-1 phr CNT-0.5 phr HAP, (c) 100 phr PVOH-2 phr CNT-0.1 phr HAP, and (d) 100 phr PVOH-2 phr CNT-0.5 phr HAP

Table 4.1: Two Theta, Crystallite Size, d-spacing, and Interchain Separation of Deflection Peak A and B for Non-Radiated Polymer Composite

Loading Level (phr)		2 Theta, 2θ (°)	Crystallite Size, L (Å)	d-spacing, d (Å)	Interchain Separation, R (Å)
CNT	HAP				
Deflection peak A					
1	0.1	19.3939	53.2689	4.5774	5.7217
1	0.5	19.6970	53.2632	4.5076	5.6345
2	0.1	20.0000	48.4441	4.4400	5.5500
2	0.5	19.6970	48.4217	4.5076	5.6345
Deflection peak B					
1	0.1	37.8913	483.4352	2.3747	2.9684
1	0.5	37.9565	644.8298	2.3708	2.9635
2	0.1	37.9565	483.5297	2.3708	2.9635
2	0.5	37.8913	552.3612	2.3747	2.9684

Table 4.2: Two Theta, Crystallite Size, d-spacing, and Interchain Separation of Deflection Peak A and B for 150 W Radiated Polymer Composite

Loading Level (phr)		2 Theta, 2θ (°)	Crystallite Size, L (Å)	d-spacing, d (Å)	Interchain Separation, R (Å)
CNT	HAP				
Deflection peak A					
1	0.1	19.6970	53.2632	4.5076	5.6345
1	0.5	19.7205	43.0875	4.5023	5.6279
2	0.1	19.6076	45.8981	4.5280	5.6600
2	0.5	19.4920	42.5525	4.5546	5.6932
Deflection peak B					
1	0.1	37.9239	644.7668	2.3727	2.9659
1	0.5	38.3700	82.5400	2.3462	2.9327
2	0.1	37.9873	125.1579	2.3689	2.9612
2	0.5	37.8772	125.5651	2.3756	2.9695

4.6 Fourier Transform Infrared (FTIR)

Figure 4.13 shows the FTIR spectra of PVOH powder, CNT powder, and HAP powder while Table A-1 shows the stretching type and its corresponding wavenumber for PVOH powder, CNT powder, and HAP powder. For PVOH powder, vibration of hydroxyl group was observed at 3283.82 cm^{-1}; stretching of CH_2 was observed at 2917.86 cm^{-1}; hydroxyl bending was observed at 1423.30 cm^{-1}; and CH bending was observed at 1323.15 cm^{-1}. It can be concluded that the tested sample is PVOH based on the existence of these four peaks. For CNT powder, vibration of hydroxyl groups

was observed at 3634.08 cm^{-1}, 3546.91 cm^{-1}, and 3366.00 cm^{-1}; stretching of CH_2 was observed at 2953.48 cm^{-1}; and vibration of carbonyl group (C=O) was observed at 1657.64 cm^{-1}. From that, the tested sample is confirmed to be CNT powder due to the presence of hydroxyl groups and carbonyl group. For HAP powder, vibration of phosphate group (PO_4^{3-}) was observed at 1060.11 cm^{-1}; and vibration of carbonate group (CO_3^{2-}) was observed at 869.83 cm^{-1}; and vibration of hydroxyl group was observed at 702.53 cm^{-1}. The tested sample is determined as HAP powder because of the three peaks where phosphate group, carbonate group, and hydroxyl group can be found.

Figure 4.14 shows the FTIR spectra of non-radiated PVOH blends while Table A-2 shows the stretching type and its corresponding wavenumber for non-radiated PVOH blends. In non-radiated sample, vibration of hydroxyl group can be observed at the wavenumber range of 3259.78-3262.59 cm^{-1}; stretching of CH_2 can be observed at the wavenumber range of 2922.39-2923.02 cm^{-1}; vibration of carbonyl group (C=O) can be observed at the wavenumber range of 1646.41-1651.71 cm^{-1}; hydroxyl bending can be observed at the wavenumber range of 1418.20-1419.08 cm^{-1}; and CH bending can be observed at the wavenumber range of 1323.26-1324.46 cm^{-1}; vibration of phosphate group (PO_4^{3-}) can be observed at the wavenumber range of 1079.27-1080.14 cm^{-1}; and vibration of carbonate group (CO_3^{2-}) can be observed at the wavenumber range of 829.03-830.37 cm^{-1}.

Figure 4.15 shows the FTIR spectra of 150 W radiated PVOH blends while Table A-3 shows the stretching type and its corresponding wavenumber for 150 W radiated PVOH blends. In 150 W radiated sample, vibration of hydroxyl group can be observed at the wavenumber range of 3259.39-3264.28 cm^{-1}; stretching of CH_2 can be observed at the wavenumber range of 2919.68-2922.67 cm^{-1}; vibration of carbonyl group (C=O) can be observed at the wavenumber range of 1649.85-1653.55 cm^{-1}; hydroxyl bending can be observed at the wavenumber range of 1419.11-1420.66 cm^{-1}; and CH bending can be observed at the wavenumber range of 1323.46-1324.38 cm^{-1}; vibration of phosphate group (PO_4^{3-}) can be observed at the wavenumber range of 1078.71-1079.33 cm^{-1}; and vibration of carbonate group (CO_3^{2-}) can be observed at the wavenumber range of 829.98-831.62 cm^{-1}.

From Figure 4.13 and Figure 4.14, the peaks of FTIR spectrum for non-radiated sample were slightly shifted as compared to the peaks of FTIR spectrum for PVOH powder, CNT powder, and HAP powder. This is because of the interaction between

PVOH, CNT, and HAP as the three materials were blended into polymer film. When comparing OH stretching of PVOH powder and OH stretching of PVOH blends, the wavenumber of OH stretching in PVOH powder (3283.82 cm^{-1}) was higher than the wavenumber of OH stretching in PVOH blends (3259.39-3264.28 cm^{-1}). This is due to the results of the "red shift" effect of hydrogen bonds. The stronger hydrogen bonds in PVOH blends weaken the bonding between oxygen atom and hydrogen atom of hydroxyl group, therefore leading to lower wavenumber of OH stretching (Tee, et al., 2013).

By comparing Figure 4.14 and Figure 4.15, it is obvious that radiated PVOH blends had one extra peak (915.97-916.72 cm-1) which did not appear in non-radiated PVOH blends. This is because microwave radiation promoted the generation of new compounds. Based on research by Qu, Zhuo, Wang, Wu, & Cheng (2018), the new absorption peaks illustrates that microwave radiation induces the formation of some polar groups. The extra peak in radiated PVOH might be attributed to the formation of polar groups under appplication of microwave radiation. Besides, it is observed that the peaks between these two figures had a very little shifting in wavenumber. From that, it is known that the microwave radiation does not change the molecular structure and composition of PVOH blends since the shifting of peaks is neglectable. This is proven by Qu, Zhuo, Wang, Wu, & Cheng (2018) that concluded microwave radiation did not affect the molecular strcuture of MWCNT when the shifting of peaks was too small to be noticed. Another research conducted by Lipka, Sienkiewicz, Gubanska, & Zalewski (2017) further proved that microwave radiation did not affect the formation of urethane bonds and chemical composition of final product.

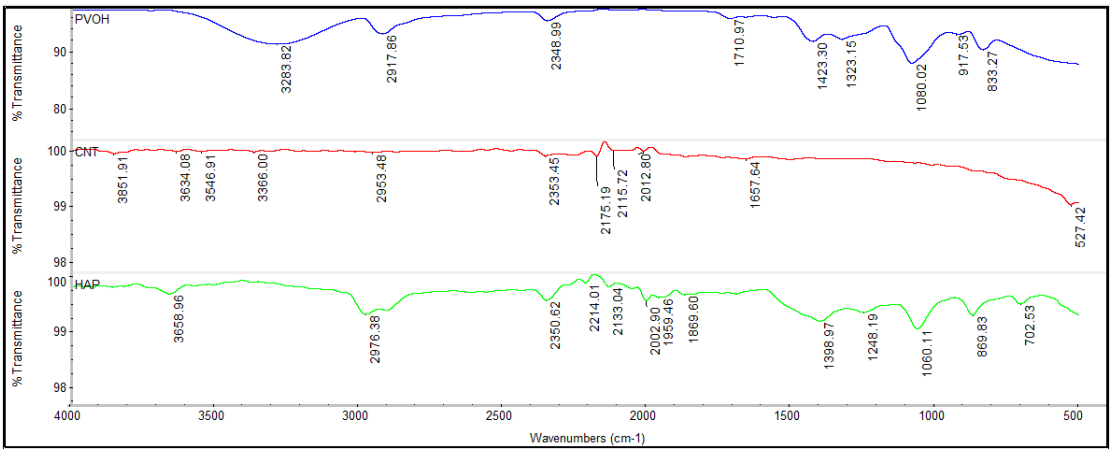

Figure 4.13: FTIR Spectrum of Powder Formed Material (PVOH, CNT, and HAP)

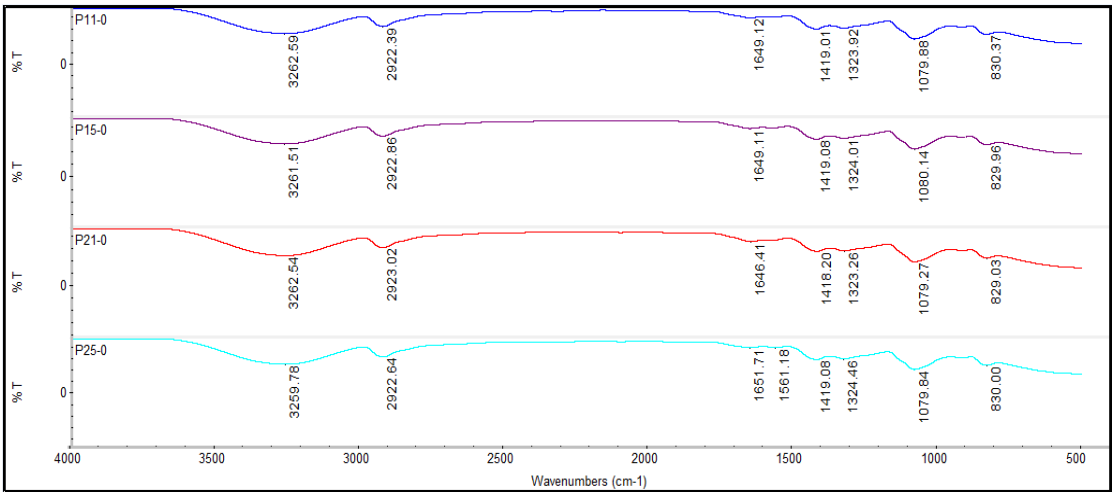

Figure 4.14: FTIR Spectrum of Non-Radiated Polymer Composite with Composition of (a) 100 phr PVOH-1 phr CNT-0.1 phr HAP, (b) 100 phr PVOH-1 phr CNT-0.5 phr HAP, (c) 100 phr PVOH-2 phr CNT-0.1 phr HAP, and (d) 100 phr PVOH-2 phr CNT-0.5 phr HAP

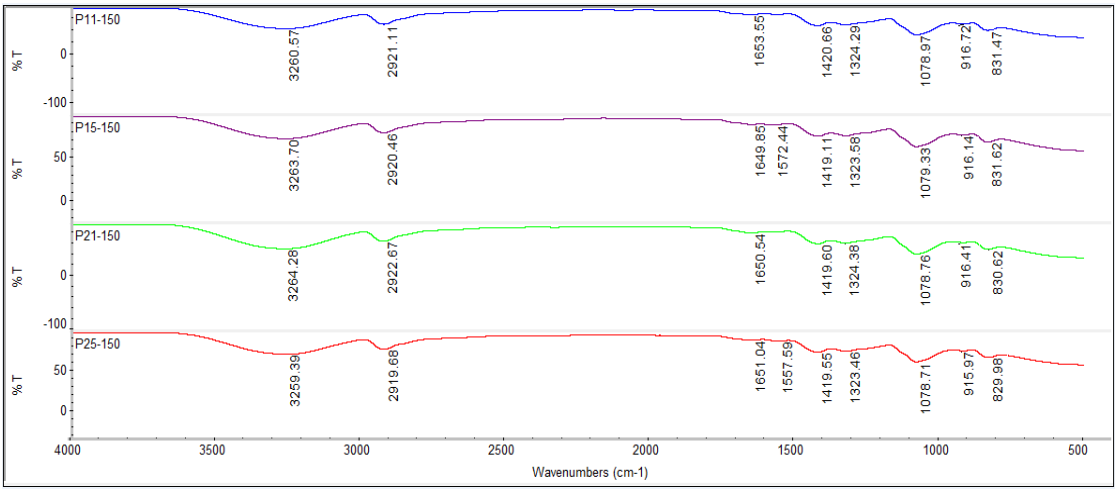

Figure 4.15: FTIR Spectrum of 150 W Radiated Polymer Composite with Composition of (a) 100 phr PVOH-1 phr CNT-0.1 phr HAP, (b) 100 phr PVOH-1 phr CNT-0.5 phr HAP, (c) 100 phr PVOH-2 phr CNT-0.1 phr HAP, and (d) 100 phr PVOH-2 phr CNT-0.5 phr HAP

4.7 Thermogravimetric Analysis (TGA)

4.7.1 Stages of Thermal Degradation

Table 4.3 illustrates the degradation temperature of three stages for non-radiated PVOH blends and 150 W radiated PVOH blends. Figure 4.16 and Figure 4.17 show the TGA curves for non-radiated PVOH blends and 150 W radiated PVOH blends. The TGA results showed that thermal degradation can be divided into three stages.

Stage 1 arose within the range of 139.54-163.35℃. In stage 1 (below 200℃), evaporation of water molecules from the polymer matrix occurs that leads to moisture loss (Mallakpour & Shafiee, 2018). The amount of moisture loss corresponding to the percentage of weight loss is determined by the physical interaction of three components (PVOH, CNT, and HAP).

Stage 2 occurred at the range of 273.83-298.69℃. In this stage (200-400℃), polymer decomposition such as breakdown of polymer backbone, decomposition of polymeric side groups, depolymerisation, and degradation of organic compounds takes place and changes the polymer structure (Sekar, et al., 2018). The decomposition is mainly due to the dehydration of vicinal hydroxyl groups with elimination of H_2O that causes the formation of conjugated unsaturated polymer chain (usually carbonyl end functional group products) (Lee, et al., 2011).

Stage 3 took place at the temperature range of 444.20-447.78℃. Stage 3 happens above 400 ℃ where C=C double bond breakdowns or polymer linkage degrades that results in production of hydrocarbon compounds such as saturated and unsaturated hydrocarbon, and cyclic hydrocarbon (Lee, et al., 2011) (Sekar, et al., 2018).

After stage 3, it can be seen that the weight loss had become constant and there is no major weight loss as temperature increases. The final weight at temperature of 900℃ is the weight of carbonaceous residues that was left behind after high thermal heating. According to Sekar, Muthukumar, Chandrasekaran, & Matheswaran (2018), the weight remained constant with increasing temperature indicates the presence of inorganic compounds.

4.7.2 Thermal Stability

Table 4.4 illustrates temperature of weight loss for non-radiated PVOH blends and 150 W radiated PVOH blends. Thermal stability of PVOH-CNT non-radiated and radiated polymer nanocomposites had reduced as HAP loading increased from 0.1 phr to 0.5 phr. This is due to the poor interfacial adhesion between HAP particles and PVOH-CNT polymer nanocomposites that triggered the breakdown of bond after the formation of weak interface zone (Yao, et al., 2013). The poor interfacial performance between HAP and PVOH blends promoted thermal degradation because of the disintegration of bond. It can be said that as loading level of HAP is increased, the interaction between HAP particles and PVOH-CNT polymer blends becomes poorer, more bonds have been disintegrated, thermal resistance of polymer nanocomposites hence decreased.

For PVOH-HAP non-radiated polymer nanocomposites, increasing CNT loading level from 1 phr to 2 phr enhanced thermal stability of polymer blends. This might be attributed to the hindering effect of CNT towards the diffusion of volatiles compounds. CNT interfered the vaporization process of some components in stage 1, this slowed down the stage 1 thermal degradation and subsequently improved the thermal stability of PVOH-HAP polymer blends. As reported by Yang, Li, Liu, Rui, & Wang (2015), thermal stability increased with higher CNT loading because of the interfering effect of CNT on diffusion of volatiles products. However for PVOH-HAP 150 W radiated polymer nanocomposite, increasing CNT loading level from 1 phr to 2 phr decreased thermal stability of polymer blends. This might be due to the application of microwave radiation at high loading level of CNT that induces chain scissioning in polymer blends, thus forming fragments of polymer. The thermal stability of PVOH-HAP 150 W radiated polymer nanocomposite at high loading of CNT had been reduced since the polymer fragments are easier to degrade under heating up to 900℃. Another factor that contributed low thermal stability is the agglomeration of CNT as CNT loading was increased and later resulted in weakening of reinforcing action of CNT. Based on research by Liu, et al. (2014), the poor dispersion effect of hydrophobic nano-particles on hydrophilic polymer formed agglomerated partcles and produced poorly developed composite. Weak developed composite was generated from poor interaction of hydrophobic CNT and hydrophilic PVOH-HAP polymer matrix, and this composite had reduced the thermal stability of polymer nanocomposite against high temperature.

It is noticed that thermal stability had improved as the PVOH-1 phr CNT-HAP polymer nanocomposites were radiated to 150 W. This is attributed to the formation of cross-linking that formed chemical bonds between polymer molecules and increasing the polymer molecular weight (Visakh, et al., 2017). The formation of chemical bonds required more energy to break down the bond, thus the thermal resistance of PVOH-1 phr CNT-HAP polymer blends had been increased. However, application of 150 W radiation reduced the thermal stability of PVOH-2 phr CNT-HAP polymer nanocomposites. This might be contributed to the high loading of CNT that allows chain scission mechanism becomes dominant over crosslinking process. As a results, this dosage of radiation on 2 phr CNT added polymer blends produced low molecular weight polymer, and exhibited low thermal stability (Visakh, et al., 2017). In short, it is observed that 100 phr PVOH-1 phr CNT-0.1 phr HAP irradiated sample had the best thermal stability among the eight polymer composites.

4.7.3 Percentage of Residue

Percentage of residue at 900℃ for non-radiated PVOH blends and 150 W radiated PVOH blends was demonstrated in Table 4.4. At temperature of 450-900℃, the weight percentage was constant for all polymer composite. There is no observable weight loss within this temperature range. The weight percent at temperature of 900℃ is the weight percent of carbonaceous char. According to Visakh, Nazarenko, Chandran, Melnikova, & Nazarenko (2017), the mechanism of the thermal stability enhancement can be contributed to barrier effect, restriction of molecular motions, and generation of protective char layer. Thus, it is known that the amount of carbonaceous char left at the end of the heating denotes the thermal stability of polymer blends.

By increasing the HAP loading level from 0.1 phr to 0.5 phr, the weight percentage of carbonaceous char had increased. For non-radiated sample, increasing CNT loading level from 1 phr to 2 phr increased the percentage of residue due to the reinforcing effect of CNT. However for 150 W radiated sample, increasing CNT loading level from 1 phr to 2 phr decreased the percentage of residue owing to the poor scattering performance of CNT at high CNT loading level.

As can be seen, 1 phr CNT radiated sample has higher percentage of residue than 1 phr CNT non-radiated sample. This is because microwave radiation that promoted cross-linking formation enable the polymer blends to have better thermal resistance. In contrast, 2 phr CNT radiated sample has lower percentage of residue

than 2 phr CNT non-radiated sample because chain scission took place and produced fragments of polymer that were poor in resisting high temperature of heating.

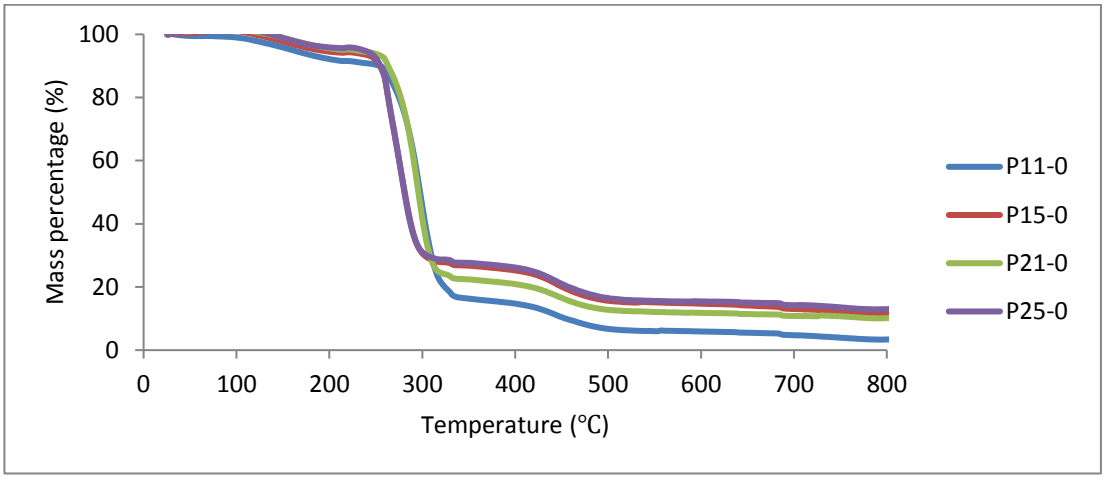

Figure 4.16: TGA Curve for Non-Radiated Polymer Composite with Composition of (a) 100 phr PVOH-1 phr CNT-0.1 phr HAP, (b) 100 phr PVOH-1 phr CNT-0.5 phr HAP, (c) 100 phr PVOH-2 phr CNT-0.1 phr HAP, and (d) 100 phr PVOH-2 phr CNT-0.5 phr HAP

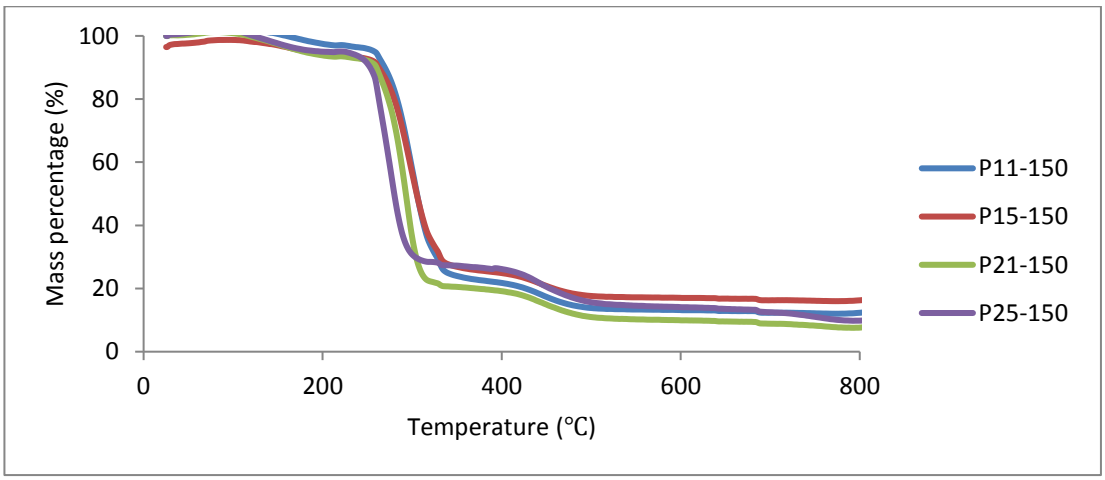

Figure 4.17: TGA Curve for 150 W Radiated Polymer Composite with Composition of (a) 100 phr PVOH-1 phr CNT-0.1 phr HAP, (b) 100 phr PVOH-1 phr CNT-0.5 phr HAP, (c) 100 phr PVOH-2 phr CNT-0.1 phr HAP, and (d) 100 phr PVOH-2 phr CNT-0.5 phr HAP

Table 4.3: Temperature of Thermal Degradation of Three Stages for Non-Radiated Polymer Composite and 150 W Radiated Polymer Composite

Sample	**Degradation Temperature (℃)**		
	1st Stage	2nd Stage	3rd Stage
P11-0	156.91	295.81	446.82
P15-0	155.43	291.42	444.20
P21-0	151.19	274.78	444.48
P25-0	149.52	274.19	444.84
P11-150	163.35	298.69	444.69
P15-150	159.07	275.40	445.64
P21-150	150.51	289.64	447.78
P25-150	139.54	273.83	447.26

Table 4.4: Temperature of Weight Loss and Percentage of Residue at 900℃ for Non-Radiated Polymer Composite and 150 W Radiated Polymer Composite

Sample	**Temperature of Weight Loss (℃)**					**Residue at 900℃ (%)**
	$T_{10\%}$	$T_{15\%}$	$T_{20\%}$	$T_{30\%}$	$T_{45\%}$	
P11-0	261.72	267.17	274.86	285.17	294.87	5.18
P15-0	254.35	260.36	263.17	269.07	278.07	13.90
P21-0	263.20	270.97	276.85	284.94	293.28	12.96
P25-0	254.90	260.52	263.34	269.31	277.91	15.80
P11-150	269.37	277.29	283.03	291.51	301.95	16.05
P15-150	262.59	272.81	279.94	289.67	301.21	19.69
P21-150	260.06	267.16	273.24	281.82	290.47	10.11
P25-150	253.03	259.75	262.78	268.76	277.22	12.93

CHAPTER 5

CONCLUSIONS AND RECOMMENDATIONS

5.1 Conclusions

This study had evaluated the effects of microwave radiation on properties of polyvinyl alcohol - carbon nanotube - hydroxyapatite blends. In short, application of microwave radiation improved mechanical and thermal properties as well as morphologies of PVOH nanocomposites but reduced crystallinity of polymer blends. Polymer blends with 2phr CNT and 0.5phr HAP exhibited the highest tensile strength, melting temperature, enthalpy of melting, d-spacing, and interchain separation. Polymer blends with 1phr CNT and 0.1phr HAP exhibited the highest crystallinity and thermal stability. Following are the conclusion made from this study:

5.1.1 Mechanical Properties

100 phr PVOH-2 phr CNT-0.5 phr HAP sample had the highest tensile strength; 100 phr PVOH-2 phr CNT-0.1 phr HAP sample had the highest Young's Modulus; and 100 phr PVOH-1 phr CNT-0.1 phr HAP had the highest elongation at break. Besides, radiated sample exhibited higher mechanical properties than non-radiated sample.

5.1.2 Thermal Properties

100 phr PVOH-2 phr CNT-0.5 phr HAP sample had the highest melting temperature and enthalpy of melting. On the other hand, radiated sample exhibited higher melting temperature and enthalpy of melting than non-radiated sample.

5.1.3 Physical Properties and Morphologies

SEM micrographs show the fractured surface morphologies of non-radiated and radiated PVOH blends. Agglomeration increased with increasing loading level of HAP or CNT. The presence of flakes was observed in 100 phr PVOH-1 phr CNT-0.5 phr HAP sample and 100 phr PVOH-2 phr CNT-0.1 phr HAP sample.

XRD results show the dispersion of filler on polymer nanocomposites and crystallinity of PVOH blends. 100 phr PVOH-2 phr CNT-0.5 phr HAP sample had the highest d-spacing and interchain separation (peak B). Radiated sample exhibited

higher d-spacing and interchain separation than non-radiated sample. However, 100 phr PVOH-1 phr CNT-0.1 phr HAP sample had the highest crystallinity. Radiated sample exhibited lower crystallinity than non-radiated sample.

5.1.4 Chemical Interactions and Bonding

For PVOH powder, vibration of hydroxyl group, stretching of CH_2, hydroxyl bending and CH bending were observed. For CNT powder, vibration of hydroxyl groups and vibration of carbonyl group (C=O) were observed. For HAP powder, vibration of phosphate group (PO_4^{3-}), vibration of carbonate group (CO_3^{2-}) and vibration of hydroxyl group were observed. The tested sample is confirmed as HAP powder because of the three peaks where phosphate group, carbonate group, and hydroxyl group can be found. For non-radiated and radiated polymer nanocomposites, the vibration of functional groups of all three powder (PVOH, CNT, and HAP) were found.

The peaks of FTIR spectrum for non-radiated sample were slightly shifted as compared to the peaks of FTIR spectrum for PVOH powder, CNT powder, and HAP powder due to the interaction between PVOH, CNT, and HAP as the three materials were blended into polymer film. The wavenumber of OH stretching in PVOH powder (3283.82 cm^{-1}) was higher than the wavenumber of OH stretching in PVOH blends (3259.39-3264.28 cm^{-1}). It is observed that the peaks between non-radiated sample and radaited sample a very little shifting in wavenumber because microwave radiation did not change the molecular structure and composition of PVOH blends.

5.1.5 Thermogravimetric Analysis

TGA results showed that thermal degradation can be divided into three stages: vaporization of water molecules, dehydration of water, and degradation. , 100 phr PVOH-1 phr CNT-0.1 phr HAP sample had the highest thermal stability. Furthermore, radiated sample exhibited higher thermal stability than non-radiated sample

5.2 Recommendations for future work

It is recommended that more tests should be carried out to better understand the properties of PVOH-CNT-HAP polymer blends. Gel content test is suggested to determine the degree of crosslinking network induced by microwave radiation. From

this test, it is easier to understand the mechanism of every polymer nanocomposites after microwave radiation.

Besides, a sample of pristine PVOH should be tested for tensile test, differential scanning calorimetry (DSC), and thermogravimetric analysis (TGA) so that it could aid in comparison of properties between pristine PVOH and PVOH blends.

Last, sample preparation step is very important because the properties of sample will depend on the preparation process. Thus, the stirring and heating of PVOH solution should be maintained at same condition in solution casting method to ensure homogeneous distribution of fillers on polymer matrix. When the solution is casting to petri dish or drying inside oven, it is recommended to place the petri dish in even surface to prevent uneven thickness of sample after drying.

REFERENCES

Aboutalebi, S. H., 2012. Advanced Energy Materials. *Enhanced hydrogen storage in graphene oxide-MWCNTs composite at room temperature,* 2(12), pp. 1439-1446.

Aussawasathien, D., He, P. & Dai, L., 2006. Polymeric nanofibers. In: *Polymer nanofibers and polymer sheathed carbon nanotubes for sensors.* s.l.:American Chemical Society Symposium Series, pp. 246-268.

Avérous, L., 2008. Monomers, Polymers and Composites from Renewable Resources. In: *Chapter 21 – Polylactic Acid: Synthesis, Properties and Applications.* Ireland: Elsevier BV, pp. 443-450.

Azahari, N. A., Othman, N. & Ismail, H., 2011. Journal of Physical Science. *Biodegradation studies of polyvinyl alcohol/corn starch blend films in solid and solution media,* Volume 22, pp. 15-31.

Bee , S. T. et al., 2018. Nuclear Inst. and Methods in Physics Research B. *Effects of electron beam irradiation on properties of corn starch undergone periodate oxidation mechanism blended with polyvinyl alcohol,* Volume 416, pp. 73-88.

Bee, S. T. et al., 2013. Nucl Instrum Math Phys Res B. *Investigation of nano-size montmorillonite on electron beam irradiated flame retardant polyethylene and ethylene vinyl acetate blends,* Volume 299, pp. 42-50.

Bee, S. T. et al., 2014. Composites: Part B. *Effects of electron beam irradiation on mechanical properties and nanostructural–morphology of montmorillonite added polyvinyl alcohol composite,* Volume 63, pp. 141-153.

Bianco, A., 2005. Current Opinion in Chemical Biology. *Applications of carbon nanotubes in drug delivery,* 9(6), pp. 674-679.

Chavan, A. A., 2015. ACS Applied Materials & Interfaces. *Elastomeric nanocomposite foams for the removal of heavy metal ions from water,* 7(27), pp. 14778-14784.

Chiellini, E., Corti, A., D'Antone, S. & Solaro, R., 2003. Progress in Polymer Science. *Biodegradation of poly (vinyl alcohol) based materials*, Volume 28, pp. 963-1014.

Chung, E. Y., 2007. Journal of Shellfish Research. *Oogenesis and sexual maturation in Meretrix lusoria (Röding 1798) (Bivalvia: Veneridae) in Western Korea*, 26(1), pp. 71-80.

Dassios, K. G. & Galiotis, C., 2012. Carbon. *Polymer–nanotube interaction in MWCNT/poly(vinyl alcohol) composite mats,* Volume 50, pp. 4291-4301.

Deepalaxmi, R. & Rajini, V., 2014. Journal of Radiation Research and Applied Sciences. *Gamma and electron beam irradiation effects on SiR-EPDM blends,* Volume 7, pp. 363-370.

DeMerlis, C. C. & Schoneker, D. R., 2003. Food and Chemical Toxicology,. *Review of the oral toxicity of polyvinyl alcohol (PVA),* 41(3), pp. 319-326.

Dorigato, A. & Pegoretti, A., 2011. Colloid and Polymer Science. *Biodegradable single-polymer composites from polyvinyl alcohol,* 290(4), pp. 359-370.

Doufnoune, R., Chebira , F. & Haddaoui, N., 2003. Int J Polym Mater. *Effect of titanate coupling agent on the mechanical properties of calcium carbonate filled polypropylene,* Volume 52, p. 967–984.

Eckel, D. F., 2004. Journal Journal. *Assessing organo-clay dispersion in polymer nanocomposites,* 93(3), pp. 1110-1117.

Fiedler, B. & Schulte, K., 2018. Comprehensive Composite Materials II. In: *Carbon Nanotube-Based Composites.* Hamburg: Elsevier Ltd, pp. 201-226.

Fombuena, V. et al., 2014. Materials and Design. *Characterization of green composites from biobased epoxy matrices and bio-fillers derived from seashell wastes,* Volume 57, pp. 168-174.

Gad, Y. H., 2009. Nucl Instrum Meth Phys Res B. *Improving the properties of poly(ethylene-co-vinyl acetate)/clay composite by using electron beam irradiation,* Volume 267, pp. 3528-3534.

Gooch, J. W., 2010. *Biocompatible Polymeric Materials and Tourniquets for Wounds.* s.l.:Springer Science & Business Media,.

Gunduz , O. et al., 2014. J Nano Mater. *A new method for fabrication of nanohydroxyapatite and TCP from the sea snail Cerithiumvulgatum,* Volume 382861, pp. 1-6.

Han, Z. & Fina, A., 2011. Progress in Polymer Science. *Thermal conductivity of carbon nanotubes and their polymer nanocomposites: a review,* 36(7), pp. 914-944.

Ishida, H., 2000. Chemistry of Materials. *General approach to nanocomposite preparation,* 12(5), pp. 1260-1267.

Ismayil, et al., 2015. Impact of electron-beam irradiation on free-volume related microstructural properties of PVA:NaBr polymer composites. *Nuclear Instruments and Methods in Physics Research B 342,* pp. 29-38.

Kaczmarska, K. et al., 2018. Spectrochimica Acta Part A: Molecular and Biomolecular. *Effect of microwave treatment on structure of binders based on sodium carboxymethyl starch: FT-IR, FT-Raman and XRD investigations,* pp. 1-22.

Karnjanapratum, S., Benjakul, S., Kishimura, H. & Tsai, Y. H., 213. Food Chemistry. *Chemical compositions and nutritional value of Asian hard clam (Meretrix lusoria) from the coast of Andaman Sea,* Volume 141, pp. 4138-4145.

Kashiwagi, M. & Hoshi, Y., 2012. SEI TECHNICAL REVIEW. *Electron beam Processing System and Its Application,* Volume 75, pp. 47-53.

Katerinopoulou, K. et al., 2014. Carbohydrate Polymers. *Preparation and characterization of acetylated corn starch–(PVOH)/clay nanocomposite films,* p. 216–222.

Kholodovych, V. & Welsh, W. J., 2007. Physical Properties of Polymers Handbook. In: J. E. Mark, ed. *Thermal-Oxidative Stability and Degradation of Polymers.* 2nd ed. New York: Springer Science , pp. 927-938.

Khonakdar, H. A., Jafari, S., Wagenknecht, U. & Jehnichen, D., 2006. Radiat. Phys. Chem.. *Effect of electron-irradiation on cross-link density and crystalline structure of low- and high-density polyethylene,* Volume 75, pp. 78-86.

Kumari, A., 2014. EXCLI Journal. *Nanoencapsulation for drug delivery,* Volume 13, p. 265.

Lee, T. S., Rahman, W. A. W. A., Rahmat, A. R. & Mokhtar , M., 2011. Carbohydrate Polymers. *Determination of thermal stability and activation energy of polyvinyl alcohol–cassava starch blends,* Volume 83, pp. 303-305.

Lewandowicz, G., Fornal, J. & Walkowski, A., 1997. Carbohydrate Polymers 34. *Effect of microwave radiation on physico-chemical properties and structure of potato and tapioca starches,* pp. 213-220.

Lewis, D. A., n.d.. IBM Corporation. *MICROWAVE PROCESSING OF POLYMERS-AN OVERVIEW.*

Lipka, J. K., Sienkiewicz, M., Gubanska, I. & Zalewski, S., 2017. European Polymer Journal 88. *Microwave radiation in the synthesis of urethane prepolymers*, pp. 126-135.

Liu, G. et al., 2014. LWT - Food Science and Technology. *Effects of nanoclay type on the physical and antimicrobial properties of PVOH-based nanocomposite films,* p. 562e568.

Mahadevaiah, Urs, T., Byrappa, K. & Somashekar, R., 2016. Procedia Engineering 141. *Effect of Microwave Irradiation on the Microstructural Properties of Bivoltine Silk Fibroin Films,* pp. 53-58.

Mallakpour, S. & Shafiee, E., 2018. Ultrasonics - Sonochemistry 40. *A simple method for the sonochemical synthesis of PVA/ZrO2-vitamin B1 nanocomposites: Morphology, mechanical, thermal and wettability investigations,* pp. 881-889.

Martin, C. A., Sandler, J. K. W. & Shaffer, M. S. P., 2004. Composites Science and Technology. *Formation of percolating networks in multi-wall carbon-nanotube–epoxy composites,* 64(15), p. 2309–2316.

Merino, S., 2015. ACS Nano. *Nanocomposite hydrogels: 3D polymer–nanoparticle synergies for on-demand drug delivery,* 9(5), pp. 4686-4697.

Mohammadi, M. et al., 2017. Radiation Physics and Chemistry. *Improvement of mechanical and thermal properties of high energy electron beam irradiated HDPE/hydroxyapatite nano-composite,* Volume 130, pp. 229-235.

Motaung, T. E. et al., 2012. Polymer Degradation and Stability. *PMMA-titania nanocomposites: Properties and thermal degradation behaviour,* Volume 97, p. 1325.

Otaguro, H. et al., 2010. Radiation Physics and Chemistry 79. *High-energy radiation forming chain scission and branching in polypropylene,* pp. 318-324.

Othman, R. N., Kinloch, I. A. & Wilkinson, A. N., 2013. Carbon. *Synthesis and characterisation of silica–carbon nanotube hybrid microparticles and their effect on the electrical properties of poly(vinyl alcohol) composites,* Volume 60, pp. 461-470.

Qian, H., Greenhalgh, E. S., Shaffer, M. S. P. & Bismarck, A., 2010. J Mater Chem. *Carbon nanotube-based hierarchical composites: a review.,* Volume 20, pp. 4751-4762.

Qu, B. et al., 2018. Composites Science and Technology 164. *Enhancement of mechanical properties of buckypapers/polyethylene composites by microwave irradiation,* p. 313–318.

Rahman, W. A. W. A.; Lee, T. S.; Rahmat, A. R.; Samad, A. A., 2010. Carbohydrate Polymers 81. *Thermal behaviour and interactions of cassava starch filled with glycerol plasticized polyvinyl alcohol blends,* pp. 805-810.

Relleve, L. S., Gallardo, A. K. R. & Abad, L. V., 2018. Radiation Physics and Chemistry 151. *Radiation crosslinking of carboxymethyl hyaluronic acid,* pp. 211-216.

Rwei , S. P. & Huang, C. C., 2012. Fibers Polym. *Electrospinning PVA solution-rheology and morphology analysis,* 13(1), pp. 44-50.

Sandler, J. K. W. et al., 2003. Polymer. *Ultra-low electrical percolation threshold in carbonnanotube-epoxy composites,* Volume 44, pp. 5893-5899.

Sanosh , K. P. et al., 2010. Met Mater Int. *Pressureless sintering of nanocrystalline hydroxyapatite at different temperatures,* Volume 16, pp. 605-611.

Sekar, A. D., Muthukumar, H., Chandrasekaran, N. I. & Matheswaran, M., 2018. Chemosphere 205. *Photocatalytic degradation of naphthalene using calcined Fe-ZnO/ PVA nanofibers,* pp. 610-617.

Shaffer, M. S. P. & Sandler, J. K. W., n.d. In: *Carbon nanotube and nanofibre reinforced polymer fibres.* London: Imperial College London, pp. 194-234.

Shaffer, W. S. P. & Windle, A. H., 1999. Adv Mater. *Fabrication and characterization of carbon nanotube /poly(vinyl alcohol) composites,* Volume 11, pp. 937-941.

Sidwell, V. D., Bonnet, J. C. & Zook, E. G., 1973. Marine Fisheries Review. *Chemical and nutritive values of several fresh and canned finfish, crustaceans, and mollusks part I: proximate composition, calcium, and phosphorus,* 35(12), pp. 16-19.

Simões, F. B. et al., n.d.. Ceramics International. *Isolated effects of microwave radiation on the solid-liquid interface reactions between hydroxyapatite nanocrystals and silver ions.*

Singh, B., Varshney, L., Francis, S. & Rajneesh, 2017. Wound Medicine 17. *Designing sterile biocompatible moxifloxacin loaded trgacanth-PVA-alginate wound dressing by radiation crosslinking method,* pp. 11-17.

Soltani , Z. et al., 2013. Radiation Physics and Chemistry. *Mechanical and thermal properties and morphological studies of 10 MeV electron beam irradiated LDPE/hydroxyapatite nano-composite,* Volume 83, pp. 79-85.

Somashekarappa, H. et al., 2013. Radiation Effects & Defects in Solids. *Effect of microwave radiation on hydroxy propyl methyl cellulose polymer films and HPMC/ poly(vinylpyrrolidone) polymer blend films using the wide-angle X-ray technique,* pp. 1-12.

Tee, T. T. et al., 2013. Composites: Part B 47. *Investigation of nano-size montmorillonite on enhancing polyvinyl alcohol-starch blends prepared via solution cast approach,* Volume 47, pp. 238-247.

Vecchio , K. S. et al., 2007. Acta Biomater. *Conversion of bulk seashells to biocompatible hydroxyapatite for bone implants,* Volume 6, pp. 910-918.

Visakh, P. M. et al., 2017. Radiation Physics and Chemistry. *Effect of electron beam irradiation on thermal and mechanical properties of aluminum based epoxy composites,* Volume 136, pp. 17-22.

Wang, B., Duan, Y., Zhang, J. & Zhao, X., 2016. Composites Part B 99. *Microwave radiation effects on carbon fibres interfacial performance,* pp. 398-406.

Wang, H. et al., 2005. Polym. Degrad. Stab.. *Transparent poly (methyl methacrylate)/silica/zirconia nanoparticles with excellent thermal stabilities,* Volume 87, p. 319.

Wang, J. H., Schertiz, D. M. & Pomplun, W. S., 1998. *Unmodified polyvinyl alcohol fibers.* US, Patent No. US6203903B1.

Wang, J., Wang, Q., Xinqing, L. & Haiqing, L., 2013. RSC Adv. *Synthesis and characterization of hydroxyapatite on hydrolyzed polyacrylonitrile nanofiber templates,* Volume 3, pp. 11132-11139.

Weerakkody, C. et al., 2018. Journal of Industrial and Engineering Chemistry. *Effects of microwave and ultrasound exposure to microsphere particles made out of different classes of inorganic and organic materials,* pp. 1-17.

Xia, M. S., Yao, Z. T., Ge, L. Q. & Chen , T., 2014. Journal of Composite Materials. *A potential bio-filler: The substitution effect of furfural modified clam shell for carbonate calcium in polypropylene,* pp. 1-10.

Xie, W. et al., 2012. Life Science Journal. *Meretrix meretrix: Activity components and their bioactivities,* 9(3), pp. 756-762.

Xie, X. L., Mai, Y. W. & Zhou , X. P., 2005. Mater Sci Eng R-Rep. *Dispersion and alignment of carbon nanotubes in polymer matrix: a review,* 49(4), pp. 89-112.

Yang, J. Q. et al., 2015. Nuclear Instruments and Methods in Physics Research B. *Effects of electron irradiation on LDPE/MWCNT composites,* Volume 365, pp. 55-60.

Yang, J. et al., 2011. Polymer. *Coorperative effect of shear and nanoclay on the formation of polar phase in poly(vinylidene fluoride) and the resultant properties,* Volume 52, pp. 4970-4978.

Yao, H. B., 2010. Angewandte Chemie International Edition. *Artificial nacre-like bionanocomposite films from the self-assembly of chitosan–montmorillonite hybrid building blocks,* 49(52), pp. 10127-10131.

Yao, Z. T. et al., 2013. Journal of Hazardous Materials. *Mechanical and thermal properties of polypropylene (PP) composites filled with modified shell waste,* Volume 262, pp. 212-217.

Yoosukh, W. & Matsukuma, A., 2001. Phuket Marine Biological Center. *Taxonomic study on Meretrix (Mollusca: Bivalvia) from Thailand,* 25(2), pp. 451-460.

Zaaba, N. F., Ismail, H. & Mariatti, M., 2016. Procedia Chemistry. *Utilization of Polyvinyl Alcohol on Properties of Recycled Polypropylene/Peanut Shell Powder Composites,* Volume 19, pp. 763-769.

APPENDICES

APPENDIX A: Fourier Transform Infrared Test (FTIR)

Table A-1: Vibration of Functional Groups for PVOH, CNT, and HAP Powder

Material	**Stretching Type**	**Wavenumber (cm^{-1})**
PVOH	OH stretching	3283.82
	CH_2 stretching	2917.86
	OH bending	1423.30
	CH bending	1323.15
CNT	OH stretching	3634.08, 3546.91, 3366.00
	CH_2 stretching	2953.48
	C=O	1657.64
HAP	PO_4^{3-}	1060.11
	CO_3^{2-}	869.83
	OH stretching	702.53

Table A-2: Vibration of Functional Groups for Non-Radiated Polymer Composite

Sample	**Stretching Type**	**Wavenumber (cm^{-1})**
P11-0	OH stretching	3262.59
	CH_2 stretching	2922.39
	OH bending	1649.12
	CH bending	1419.01
	C=O	1323.92
	PO_4^{3-}	1079.88
	CO_3^{2-}	830.37
P15-0	OH stretching	3261.51
	CH_2 stretching	2922.86
	OH bending	1649.11
	CH bending	1419.08
	C=O	1324.04
	PO_4^{3-}	1080.14
	CO_3^{2-}	829.96
P21-0	OH stretching	3262.54
	CH_2 stretching	2923.02
	OH bending	1646.41
	CH bending	1418.20
	C=O	1323.26
	PO_4^{3-}	1079.27
	CO_3^{2-}	829.03
P25-0	OH stretching	3259.78
	CH_2 stretching	2922.64
	OH bending	1651.71
	CH bending	1419.08
	C=O	1324.46
	PO_4^{3-}	1079.84
	CO_3^{2-}	830.00

Table A-3: Vibration of Functional Groups for 150 W Radiated Polymer Composite

Sample	**Stretching Type**	**Wavenumber (cm^{-1})**
P11-150	OH stretching	3260.57
	CH_2 stretching	2921.11
	OH bending	1653.55
	CH bending	1420.66
	C=O	1324.29
	PO_4^{3-}	1078.97
	CO_3^{2-}	831.47
P15-150	OH stretching	3263.70
	CH_2 stretching	2920.46
	OH bending	1649.85
	CH bending	1419.11
	C=O	1323.58
	PO_4^{3-}	1079.33
	CO_3^{2-}	831.62
P21-150	OH stretching	3264.28
	CH_2 stretching	2922.67
	OH bending	1650.54
	CH bending	1419.60
	C=O	1324.38
	PO_4^{3-}	1078.76
	CO_3^{2-}	830.62
P25-150	OH stretching	3259.39
	CH_2 stretching	2919.68
	OH bending	1651.04
	CH bending	1419.55
	C=O	1323.46
	PO_4^{3-}	1078.71
	CO_3^{2-}	829.98